NANOscientific

ISSUE NO. 16

The Magazine for NanoScience and Technology

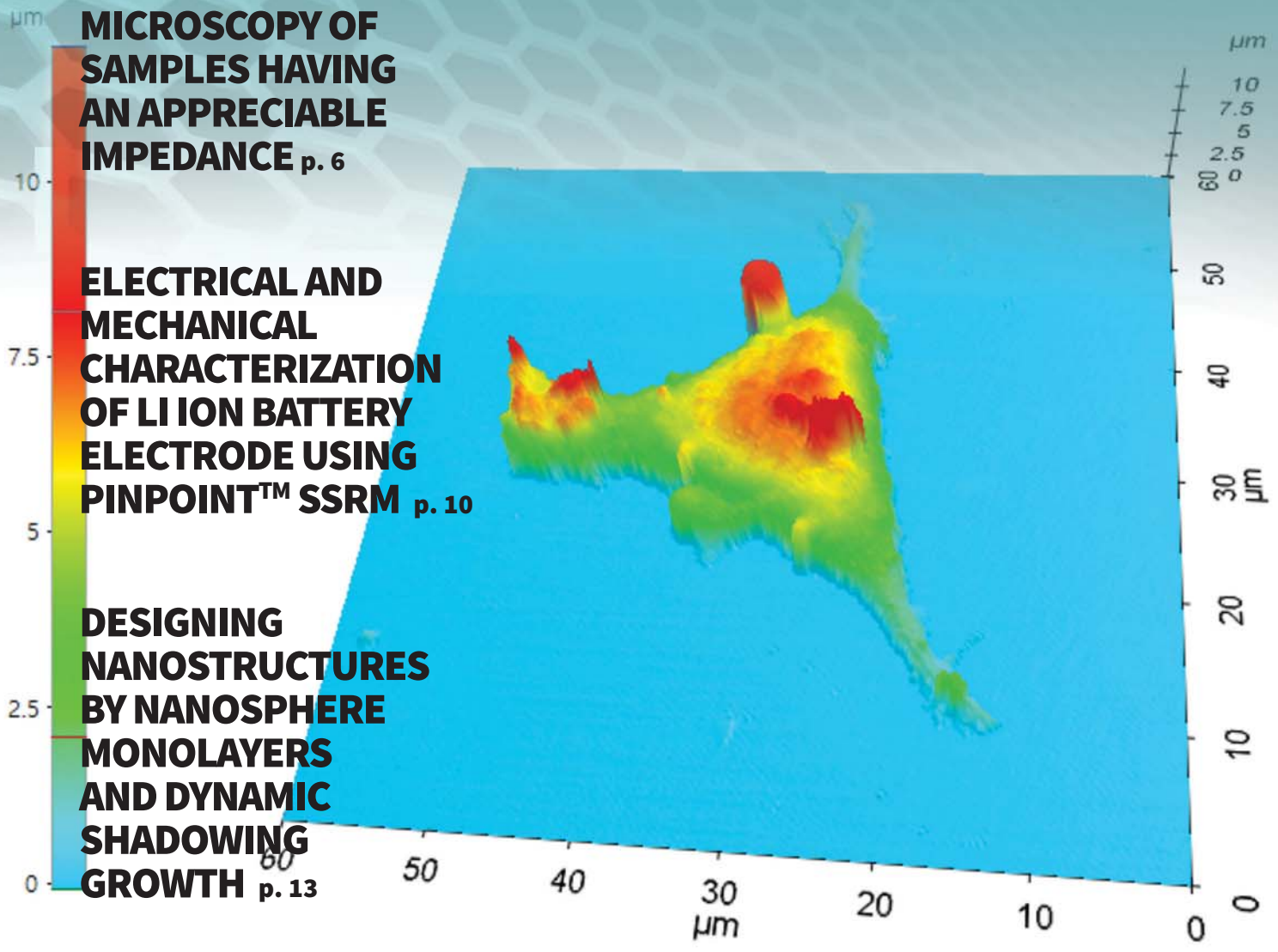

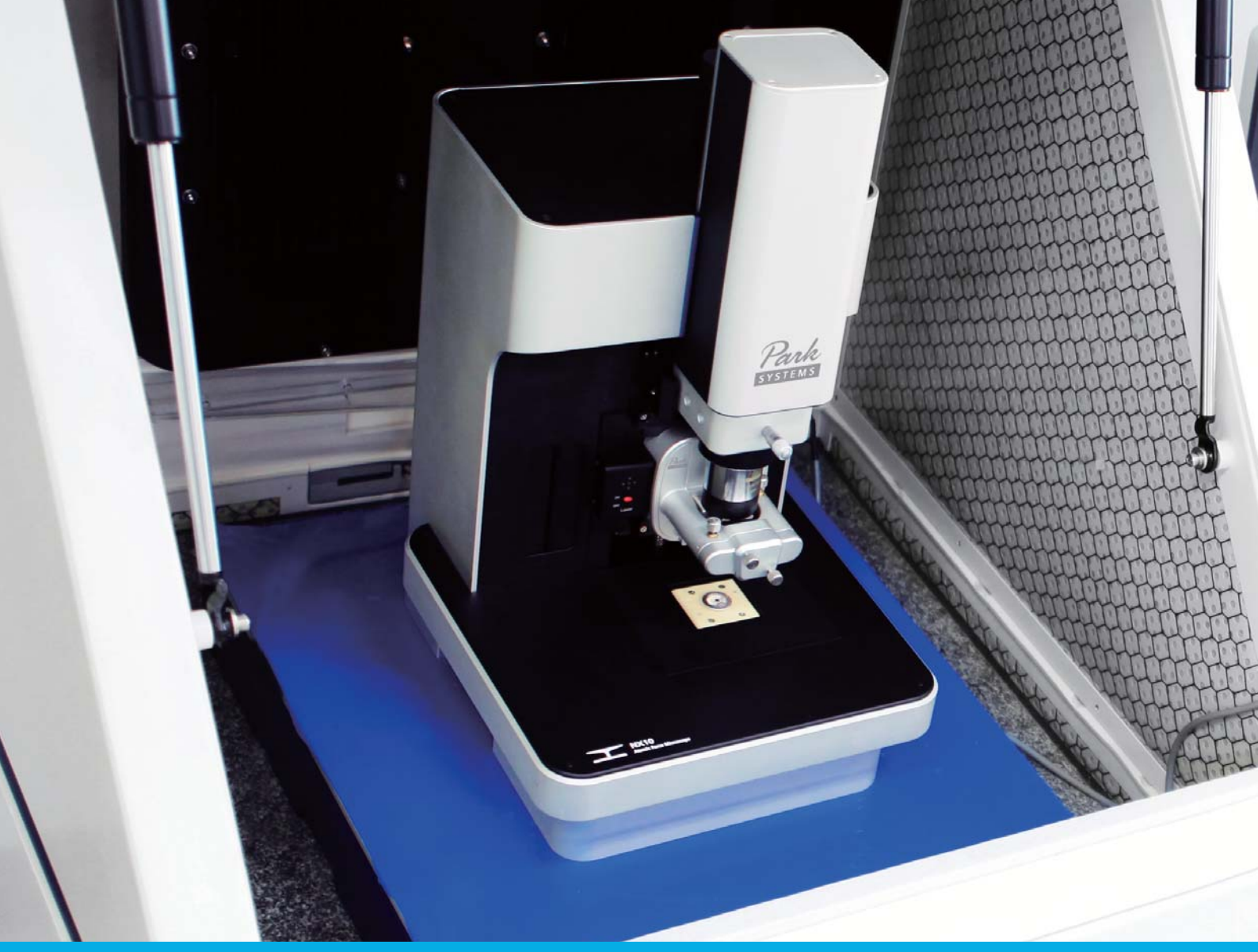

Park NX10 the quickest path to innovative research

Better accuracy means better data

Park NX10 produces data you can trust, replicate, and publish at the highest nano resolution. It features the world's only true non-contact AFM that prolongs tip life while preserving your sample, and flexure based independent XY and Z scanner for unparalleled accuracy and resolution.

Better accuracy means better productivity

From sample setting to full scan imaging, measurement, and analysis, Park NX10 saves you time every step of the way. The user friendly interface, easy laser alignment, automatic tip approach, and analysis software allow you to get publishable results faster.

Better accuracy means better research

With more time and better data, you can focus on doing more innovative research. And the Park NX10's wide range of measurement modes and customizable design means it can be easily tailored to the most unique projects.

www.parksystems.com

inquiry@parksystems.com

The Most Accurate Atomic Force Microscope

Park SYSTEMS

TABLE OF CONTENTS

NanoScientific Issue No. 16

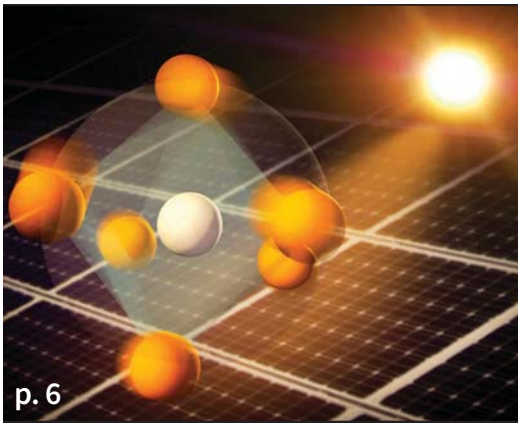

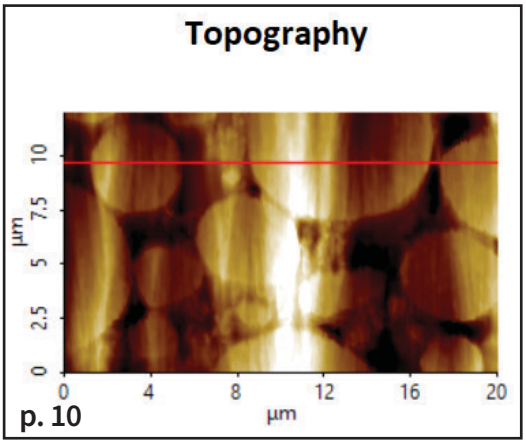

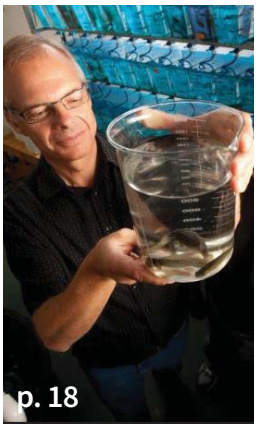

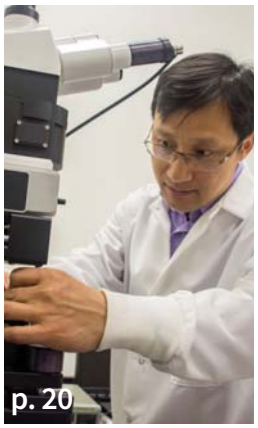

NANOscientific

Keibock Lee, Editor-in-Chief
kei@nanoscientific.org

Deborah West, Content Editor
debbiewest@nanoscientific.org

Debbie Bishop, Art Director

Published by Park Systems, Inc.
3040 Olcott St.
Santa Clara, CA 95054
inquiry@parksystems.com
408-986-1110

www.parkystems.com

NANOScientific is published quarterly to showcase advancements in the field of nanoscience and technology across a wide range of multidisciplinary areas of research. The publication is offered free to anyone who works in the field of nanotechnology, nanoscience, microscopy and other related fields of study and manufacturing.

We would enjoy hearing from you, our readers. Send your research or story ideas to **debbiewest@nanoscientific.org**

To view all of our articles, please visit our web site at **www.nanoscientific.org.**

INSET PHOTO ON COVER:

This image was produced using scanning ion conductance microscopy of Park Systems. In this figure, 80 nm of inner diameter nano-pipette was used for high resolution cell surface imaging. The imaging size is 60 x 60 um with 256 x 256 pixel resolution, enough to display a single cell. The approach-retract scanning (ARS) mode was used to obtain a reliable and stable image of a whole single cell.

Park SYSTEMS

Keibock Lee, Editor-in-Chief

NANOSCIENTIFIC ANNOUNCES NEW EDITORIAL BOARD FOR 2019

NanoScientific is pleased to announce they have selected a new Editorial Board for 2019 which will be responsible for peer reviews of papers submitted for consideration and offer counsel on content for the publication. We are proud to welcome the 2019 NanoScientific Editorial Board members.

MESSAGE FROM EDITOR

Welcome to the NanoScientific Editorial Board

I would like to take this opportunity to officially welcome the first NanoScientific Editorial Board. Since 2014, NanoScientific has been publishing original research papers and application notes, news, and engaging interviews on emerging Nano Science and Technology, with a strong emphasis on interdisciplinary issues reflecting the complex relationship between Nano Materials and Nano Metrology.

This year, with the formation of an official editorial board, we will be able to peer review submitted articles, in order to maintain the highest standards of quality.

The editorial board members and the peer-reviewing process will help NanoScientific become a key platform for the exchange of peer-reviewed global information in pursuit of scientific knowledge sharing world-wide. As editor-in-chief, I am delighted that they have become a part of NanoScientific and look forward to their contributions to the journal.

We are actively looking for presenters at our NanoScientific Symposium in 2019 and for contributed articles for our NanoScientific Journal. Presenters will have first priority for published papers. Please submit your abstract for consideration to debbiewest@nanoscientific.org.

Keibock Lee
Editor-in-Chief

NanoScientific Symposiums in 2019

Bologna Italy- Sept. 11-13, 2019 Albany NY-Nov. 13-14, 2019
Mexico City Oct. 3-4, 2019

NanoScientific 2019 Editorial Board


Dr. Rigoberto Advincula, Professor, Department of Macromolecular Science and Engineering at Case Western Reserve University.


Dr. Lane Baker, James L. Jackson Professor of Chemistry Indiana University


Mr. Phil Kaszuba, Global Foundries Senior Member of Technical Staff and lead engineer in their Scanning Probe Microscopy (SPM) laboratory.


Dr. John A. Marohn, Professor & Director of Undergraduate Studies,Department of Chemistry and Chemical Biology Member, Field of Materials Science & Engineering,Cornell University.


Dr. Ye Tao, Rowland Fellow & Principle Investigator, Rowland Institute of Science at Harvard University, BA Harvard in Biochemistry, PhD MIT/ ETH Zurich Chemistry

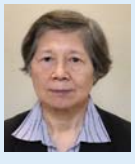
Dr. Gwo-Ching Wang, Travelstead Institute Chair, Dept. of Physics, Applied Physics & Astronomy, Rensselaer Polytechnic Institute.

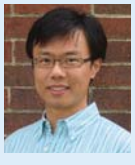
Dr. Jiahua Jack Zhu, PhD, University of Akron, Associate Professor, Department of Chemical and Biomolecular Engineering.


Dr. Yiping Zhao Professor, Department of Physics and Astronomy, Director, Nanoscale Science and Engineering Center, The University of Georgia.

FEATURE ARTICLE

ELECTRIC FORCE MICROSCOPY OF SAMPLES HAVING AN APPRECIABLE IMPEDANCE

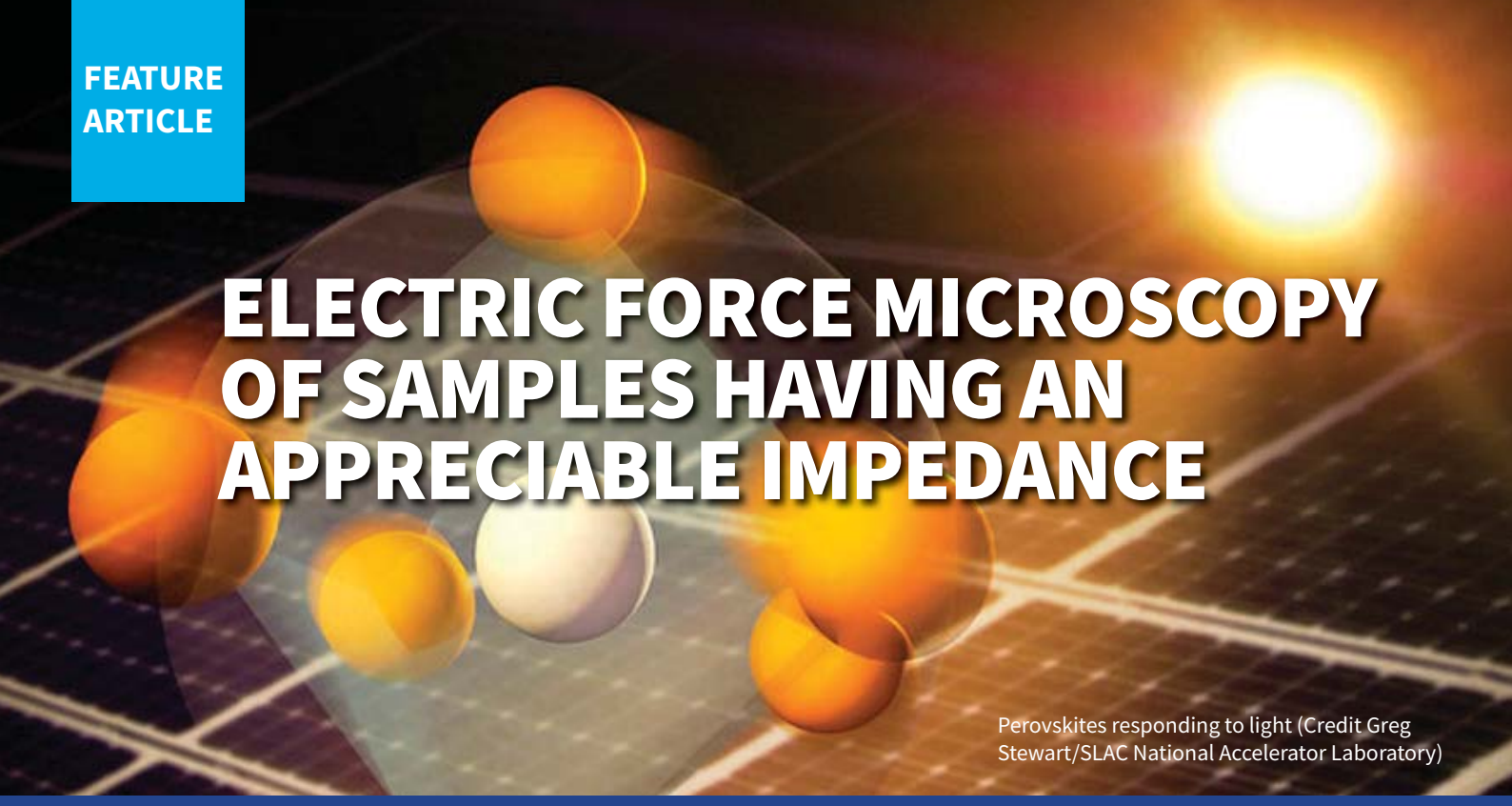

Perovskites responding to light (Credit Greg Stewart/SLAC National Accelerator Laboratory)

Ryan P. Dwyer[1,2], John A. Marohn[1]

Summary

KPFM experiments are used to image capacitance and surface potential in a wide variety of samples. The widely used KPFM frequency-shift equation rests on assumptions that are questionable in samples having an appreciable impedance or properties that evolve on a fast timescale. We present new equations describing the cantilever frequency and dissipation in a KPFM experiment carried out on a sample with an appreciable stationary or time-dependent impedance, such as a photovoltaic film, a battery material, or mixed electronic-ionic conductors.

Article

Scanned probe microscopy (SPM) techniques that measure electrostatic forces have revealed the fate of charges in a broad array of semiconductor electronic and photovoltaic devices. The equation commonly used to interpret frequency-modulated scanning Kelvin probe force microscopy (KPFM) measurements of electric forces is

$$\Delta f = -\frac{f_0}{4k_0} C'' (V_{ts} - \Phi)^2 , \qquad (1)$$

where Δf is the time-dependent cantilever frequency shift, f_0 is the cantilever resonance frequency, k_0 is the cantilever spring constant, C'' is the second derivative of the tip-sample capacitance with respect to the vertical direction, V_{ts} is the applied tip-sample voltage, and Φ is the sample surface potential. Recent experiments have called the validity of this equation into question.

Figure 1 shows one striking example.[1] The sample was a thin film of the perovskite semiconductor $CsPbBr_3$ prepared on a conductive indium tin oxide substrate, illuminated from above with visible light (Fig. 1(a)). The cantilever frequency shift and amplitude were measured at different applied tip-sample voltages to determine the curvature of the frequency- and dissipation-versus-voltage parabolas (Fig. 1(b)). Figure 1(c) and (d) show how these parabola curvatures depend on the light intensity.

According to Eq. 1, the curvature of the frequency-shift-versus-voltage parabola is proportional to the tip-sample capacitance derivative C'', which in turn should be proportional to the free carrier density. In a semiconductor, this free carrier density has a power-law-dependence on the light intensity. The capacitance data, in contrast, increases rapidly but then flattens out as the light intensity is increased. Likewise, the dissipation should increase linearly with the carrier density. The experimental data contradicts this prediction even more dramatically, showing a sharp peak in dissipation at moderate light intensity, and decreasing dissipation at high light intensities, even as the free carrier density surely continues to increase.

The source of these apparent contradictions is not the sample or the microscope, but Eq. 1. The problem lies in two hidden, seldom-stated assumptions needed to derive Eq. 1. The two assumptions are

1. the tip charge oscillates exactly in phase with the cantilever motion to keep the tip voltage constant, and
2. any changes in the tip-sample interaction happen slowly.

In the Fig. 1 experiment, the problem is that the increased dissipation implies a tip charge oscillating out of phase with the cantilever motion — a clear violation of assumption 1.

To move forward, we needed a model that describes the cantilever frequency shift and dissipation even when these assumptions are violated. We use Lagrangian mechanics to describe the coupled motion of cantilever tip displacement, tip charge, and sample charge. Based on its usefulness in electrochemical impedance spectroscopy, we describe the sample using a complex impedance. Using this new model, we derived two equations that *replace* Eq. 1.

[1]Department of Chemistry and Chemical Biology; Cornell University; Ithaca, New York 14853 [2]Department of Chemistry and Biochemistry; University of Mount Union; Alliance, Ohio 44601

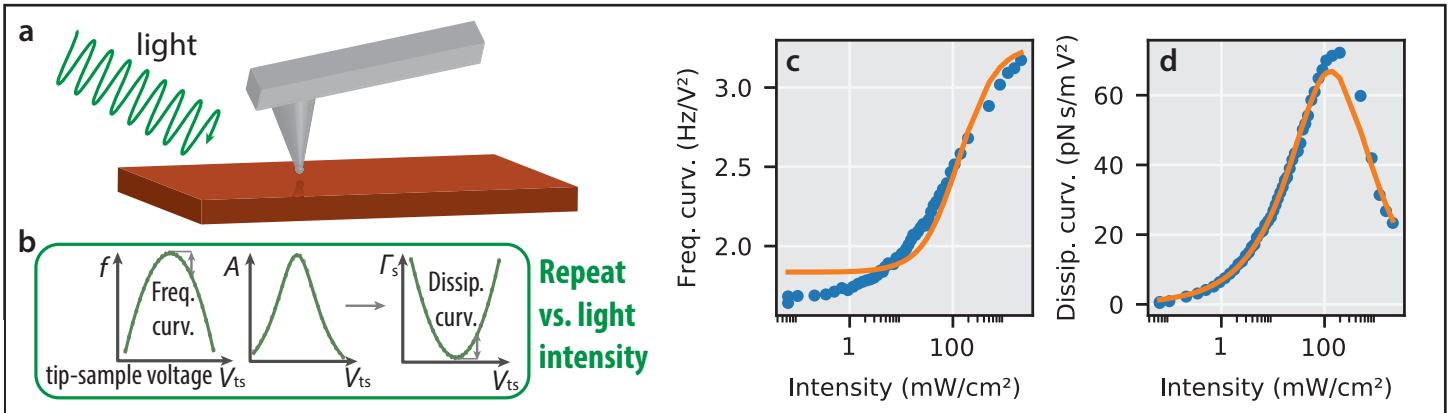

Figure 1. Apparent violation of Eq. 1 in an illuminated thin-film semiconductor, $CsPbBr_3$. Modified from Tirmzi et al., 2017, ACS Energy Lett.; copyright American Chemical Society.[1]

The frequency shift is

$$\Delta f = -\frac{f_0}{4k_0}\left(C_q'' + \Delta C'' \,\mathrm{Re}\left(\hat{H}(\omega_0)\right)\right)V^2 \qquad (2)$$

and the sample-induced dissipation is

$$\Gamma_s = -\frac{1}{4\pi f_0}\Delta C'' \,\mathrm{Im}\left(\hat{H}(\omega_0)\right)V^2, \qquad (3)$$

with $= 2(C')^2/C$ and $C_q'' = C'' - \Delta C''$ two distinct capacitance derivatives, and

$$\hat{H}(\omega) = \frac{1}{1 + j\omega C Z(\omega)} \qquad (4)$$

the transfer function between the applied tip-sample voltage and the tip voltage drop, which depends on the tip capacitance C and the complex sample impedance $Z(\omega)$. These two equations should replace Eq. 1 whenever the tip charge does not oscillate exactly in phase with the cantilever motion.

To explain the data of Fig. 1, we model the sample as a capacitor C_s and light-dependent resistor R_s operating in parallel (Fig. 2(a)). The central new quantity is $\hat{H}(\omega_c)$, the transfer function evaluated at the cantilever resonance frequency. Figure 2(b) shows that the transfer function has a roll-off frequency determined by the time constant $\tau = R_s(C+C_s) \approx R_s C_s$. The real part of the transfer function H' causes a force F' oscillating in phase with the cantilever motion which results in a cantilever frequency shift Δf (Fig. 2(c)). The imaginary part of the transfer function H'' causes a force F'' oscillating out of phase with the cantilever motion which results in sample-induced dissipation — this is the component of the tip-sample interaction completely neglected in Eq. 1 (Fig. 2(d)). We can explain the dramatic peak in dissipation by assuming R_s is large in the dark and small under illumination. The peak in dissipation occurs at an illumination intensity where τ^{-1} equals the cantilever frequency ω_0.

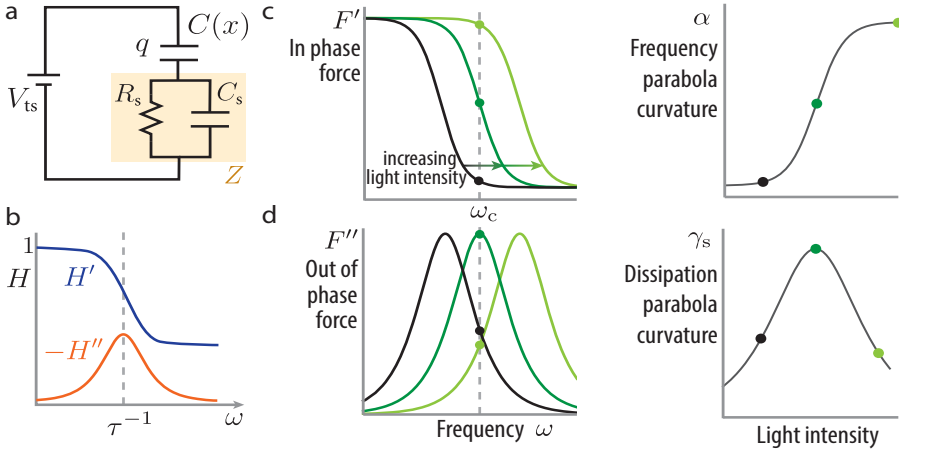

Figure 2. A Lagrangian-impedance treatment of the tip-sample interaction and a parallel-RC model of the sample explains the seemingly anomalous results of Fig. 1. Modified from Tirmzi et al., 2017, ACS Energy Lett.; copyright American Chemical Society[1]

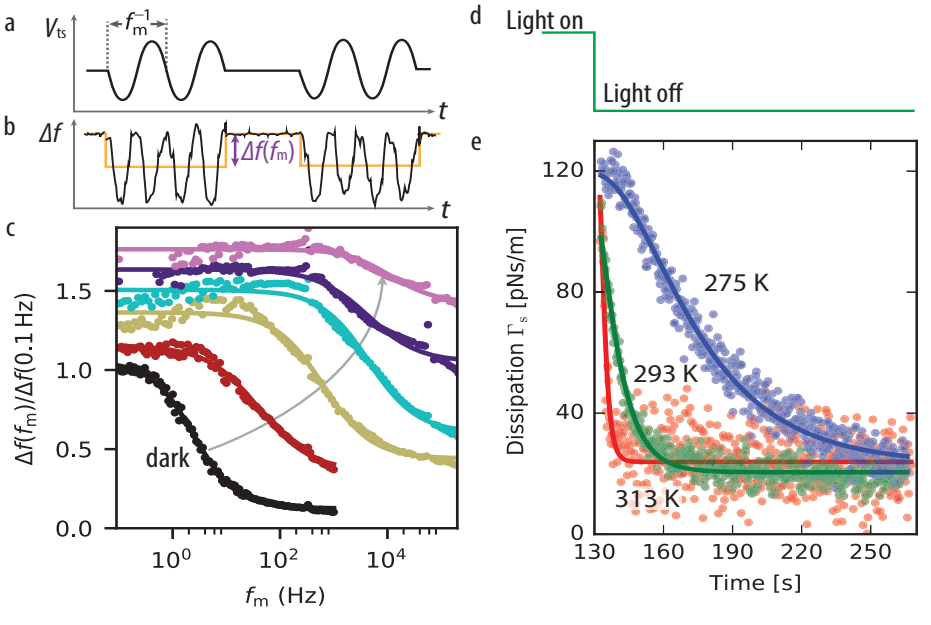

Figure 3. The Lagrangian-impedance model provides a framework for interpreting (a–c) broadband local dielectric spectroscopy, and (d–e) cantilever ringdown dissipation measurements. Modified from Tirmzi et al., 2017, ACS Energy Lett.; copyright American Chemical Society.[1]

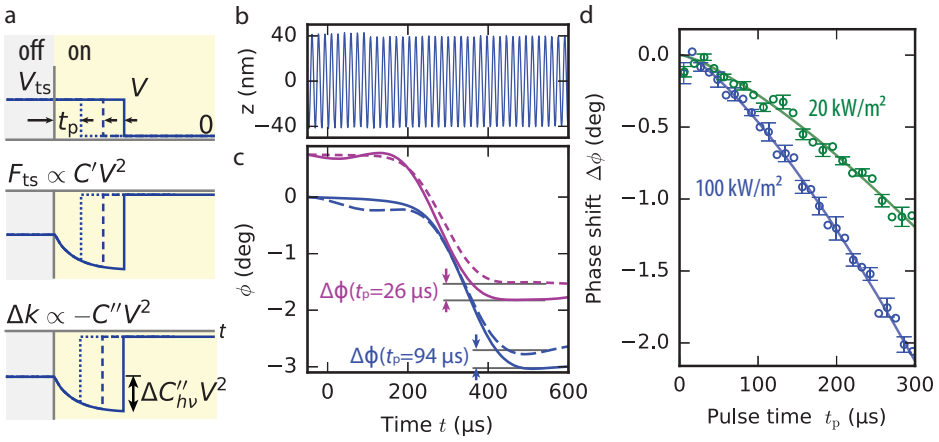

Figure 4. Phasekick electric force microscopy accurately measures light-induced changes in the tip-sample interaction even when the light or voltage induces abrupt changes in the tip-sample interaction, in violation of assumption 2. Modified from Dwyer et al., 2017, Sci. Adv.; copyright American Association for the Advancement of Science, CC BY-NC 4.0.[9]

The lines in Fig. 1(c,d) are a fit of the data to Eqs. 2 and 3. The joint fit nicely captures the nonlinear behavior of both the frequency and the dissipation versus illumination intensity.

This new model of the tip-sample interaction connects and integrates the results of a wide variety of scanned probe experiments. Figure 3(a–c) shows a broadband local dielectric spectroscopy measurement[2] carried out on the $CsPbBr_3$ film of Fig. 1. The measured quantity is the difference in cantilever frequency shift caused by modulating the tip-voltage at a frequency f_m. According to our Lagrangian-impedance model, this experiment mainly measures the real part of the transfer function at the modulation frequency $H'(f_m)$. The change in the spectrum's knee with increasing light intensity is in qualitative agreement with the light-dependent R_s used to explain the Fig. 1 data, validating the use of a relatively simple RC sample impedance model to explain a wide range of experiments carried out on the photovoltaic $CsPbBr_3$ sample.

To gain a better understanding of the microscopic origin of this light-dependent resistance R_s in $CsPbBr_3$, we examined the kinetics of the resistance recovery in the dark at different temperatures. Figure 3(e) shows measurements of the sample-induced dissipation inferred from repeated cantilever ringdown measurements acquired just after turning off the light. The increased dissipation, caused by a reduction in the sample resistance R_s, decreases slowly with a time constant ranging from 2 seconds at 313 K to over 30 seconds at 275 K. An Arrhenius plot shows that the process by which the resistance goes back to its dark value is highly activated, with an activation energy E_a=0.52±0.03 eV. This slow, highly activated process rules out many simple explanations of the sample-induced resistance[3,4] and supports the suggestion that light creates mobile ionic vacancies in $CsPbBr_3$.[5] The Lagrangian-impedance model links each experiment shown in Figs. 1 and 3 back to the sample impedance $Z(\omega)$, allowing the experiments to be interpreted in a common framework.

Figures 1–3 show that the Lagrangian-impedance model helps us interpret results when the assumption that the tip charges oscillates exactly in phase with the cantilever is violated (assumption 1). What about the other assumption, that any changes in the tip-sample interaction occur slowly? This assumption can be violated in electric force microscopy (EFM) experiments that follow the time evolution of photocapacitance in response to illumination.[6-8] These experiments have pushed the limits of time resolution in electric force microscopy, with claimed time resolutions down to less than 1 percent of the cantilever period.[8] Our analysis shows that the standard equation for frequency shift in KPFM cannot be used to analyze these single-shot, transient EFM experiments because the abrupt changes in the tip-sample force shift the cantilever's amplitude and phase.

Biographical sketches

John Marohn earned a B.S. in Chemistry and a B.A. in Physics from the University of Rochester. His Chemistry Ph.D. research was carried out at the California Institute of Technology under the mentorship of Daniel Weitekamp. He did postdoctoral work at the U.S. Army Research Laboratory with Doran Smith as a U.S. National Research Council Postdoctoral Associate. In 1999 he joined the faculty at Cornell University, where he is presently a Professor of Chemistry and Chemical Biology, serves as his department's Director of Undergraduate Studies, is a member of the Cornell Center for Materials Research, and is a member of Cornell's graduate field of Materials Science and Engineering. In 2006, Professor Marohn created the 1st International Conference on nanometer-scale Magnetic Resonance Imaging; the 6th International nano-MRI conference was held in February 2018. In 2012 he landed a Ruth L. Kirschstein National Research Service Award from the National Institutes of Health that allowed him to work for a year as a visiting scientist at The Scripps Research Institute in La Jolla, California. His research group has three themes: (1) developing a microscopic view of organic and hybrid electronic materials using high-sensitivity electric force microscopy, (2) performing nanoscale magnetic resonance imaging using mechanical detection, and (3) studying near-surface fluctuations using microcantilevers.

Ryan Dwyer earned a B.S. in Chemistry from the University of Notre Dame. His chemistry Ph.D. research was performed with John Marohn at Cornell University. He is presently an Assistant Professor of Chemistry and Biochemistry at University of Mount Union where he teaches general and physical chemistry.

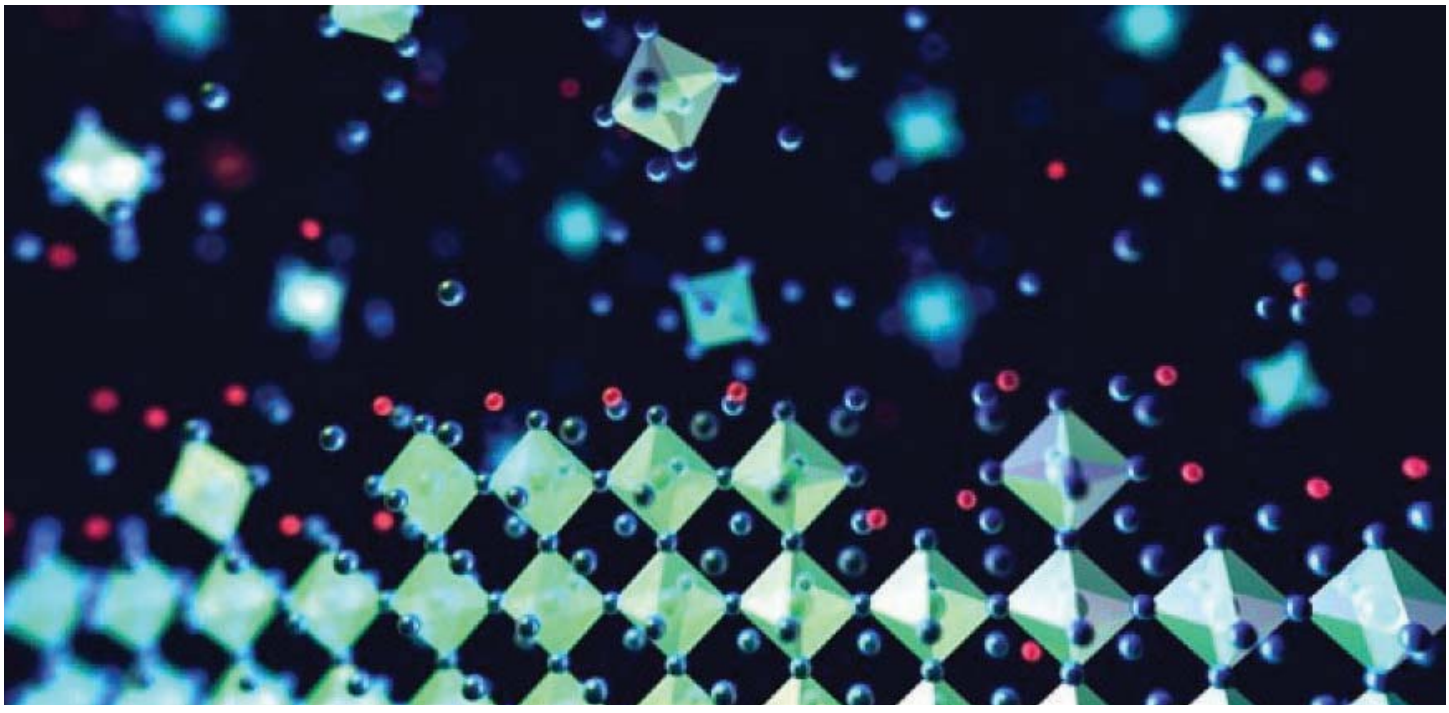

Atomic scale view of Perovskite crystal formation. Credit: Matt Klug

The Lagrangian formalism, however, can be used to interpret these results and design experiments that accurately measure abrupt changes in the tip-sample interaction.

The phasekick electric force microscopy experiment sketched in Fig. 4 shows how. The light is turned on at time t=0, inducing a possibly abrupt change in the capacitance. The voltage is turned to zero abruptly at a time t_p (Fig. 4(a)). We infer the light-induced phase shift as a function of the stepped pulse time t_p (Fig. 4(b)). Representative data at two pulse times is shown in Fig. 4(c). A photocapacitance-induced phase shift is computed by comparing relative phase-shift data in the dark (dashed line) and under illumination (solid line). Figure 4(d) shows representative phase-shift versus pulse-time data acquired for 768 pulse times at two different light intensities over a polymeric solar-cell film. In Ref. 9, analyzing the Fig. 4(d) data revealed that the photovoltaic sample's photocapacitance had biexponential dynamics.

The Lagrangian-impedance approach to understanding electric force microscopy highlighted here has a number of advantages. It accounts for dissipation of energy in both the sample and the cantilever; treats both steady-state and transient phenomena in a unified way; and captures the effects of sub-cycle changes in sample capacitance, conductivity, and tip charge that are missing from previous treatments of the cantilever-sample interaction in EFM and KPFM. The Lagrangian-impedance point of view has inspired new measurements and has forced us to rethink established measurements. The phasekick EFM measurement of Fig. 4 enables the measurement of sample charge motion on a timescale much shorter than even a single cantilever period. The assumptions underlying Eq. 1 are questionable in many interesting samples. Equations 2 through 4 should be used in place of Eq. 1 in any frequency-modulated KPFM experiment carried out on a sample with appreciable impedance, including photovoltaic films, battery materials, and mixed electronic-ionic conductors.

Methods

The data in Figs. 1, 3, and 4 were acquired on a custom-built vacuum/variable-temperature scanned probe microscope in Marohn's laboratory at Cornell.

Acknowledgements

The authors acknowledge financial support from the U.S. National Science Foundation (Grant DMR-1709879).

References

[1] A. M. Tirmzi, R. P. Dwyer, T. Hanrath, and J. A. Marohn, Coupled slow and fast charge dynamics in cesium lead bromide perovskite, ACS Energy Lett., 2017, 2, 488 – 496, URL http://dx.doi.org/10.1021/acsenergylett.6b00722.

[2] M. Labardi, M. Lucchesi, D. Prevosto, and S. Capaccioli, Broadband local dielectric spectroscopy, Appl. Phys. Lett., 2016, 108, 182906, URL http://dx.doi.org/10.1063/1.4948767.

[3] A. M. Tirmzi, J. A. Christians, R. P. Dwyer, D. T. Moore, and J. A. Marohn, Substrate-dependent photoconductivity dynamics in a high-efficiency hybrid perovskite alloy, J. Phys. Chem. C, 2019, 123, 3402 – 3415, URL http://dx.doi.org/10.1021/acs.jpcc.8b117832019.

[4] R. P. Dwyer, L. E. Harrell, and J. A. Marohn, Lagrangian and impedance spectroscopy treatments of electric force microscopy, Phys. Rev. Appl. (in press), 2019, URL https://arxiv.org/abs/1807.01219.

[5] G. Y. Kim, A. Senocrate, T.-Y. Yang, G. Gregori, M. Grätzel, and J. Maier, Large tunable photoeffect on ion conduction in halide perovskites and implications for photodecomposition, Nat. Mater., 2018, 17, 445 – 449, URL http://dx.doi.org/10.1038/s41563-018-0038-0.

[6] D. C. Coffey and D. S. Ginger, Time-resolved electrostatic force microscopy of polymer solar cells, Nat. Mater., 2006, 5, 735 – 740, URL http://dx.doi.org/10.1038/nmat1712.

[7] R. Giridharagopal, G. E. Rayermann, G. Shao, D. T. Moore, O. G. Reid, A. F. Tillack, D. J. Masiello, and D. S. Ginger, Submicrosecond time resolution atomic force microscopy for probing nanoscale dynamics, Nano Lett., 2012, 12, 893 – 898, URL http://dx.doi.org/10.1021/nl203956q.

[8] D. U. Karatay, J. S. Harrison, M. S. Glaz, R. Giridharagopal, and D. S. Ginger, Fast time-resolved electrostatic force microscopy: Achieving sub-cycle time resolution, Rev. Sci. Instrum., 2016, 87, 053702, URL http://dx.doi.org/10.1063/1.4948396.

[9] R. P. Dwyer, S. R. Nathan, and J. A. Marohn, Microsecond photocapacitance transients observed using a charged microcantilever as a gated mechanical integrator, Sci. Adv., 2017, 3, e1602951, URL http://dx.doi.org/10.1126/sciadv.1602951.

APPLICATION NOTE

ELECTRICAL AND MECHANICAL CHARACTERIZATION OF LI ION BATTERY ELECTRODE USING PINPOINT™ SSRM

John Paul Pineda, Cathy Lee, Byong Kim, and Keibock Lee
Park Systems Inc., Santa Clara, CA USA

Introduction

Lithium ion batteries (LIBs) are key components of modern electronics and are regularly utilized as their primary power source [1-3]. LIBs have become ubiquitous in a variety of applications ranging from portable devices to electric vehicles because of their high energy density, flexible and lightweight design, lower self-discharge, low cost and longer lifespan compared to other battery technologies [4,11]. Despite these advantages, the reliability and performance of LIBs still need to be improved to meet the requirements of applications such as large-scale energy storage and hybrid electric vehicles (HEV) [2,5,11]. Extensive research has focused on the development of four cell materials in particular to achieve better performance: positive and negative electrode active materials (AM) as well as separators and electrolytes [2]. Understanding the electrical and mechanical properties of electrode materials plays a major role in the performance improvement of LIBs. It has been shown that improved adhesions between electrode particles, and between electrode films and current collectors lead to better retention of discharge capacity during cycling, especially when electrode materials exhibit faster and/or larger volume expansion [2]. Moreover, enhanced electronic conductivities and ionic diffusivities in electrodes also lead to LIB capacity improvements [6]. As devices become more compact, optimizing electrical and mechanical properties on a nanometer scale gets more relevant and leads to improved interfaces.

There are several methods that can measure these local properties; the more common methods include impedance spectroscopy and nanoindentation [3,7,8]. However, even when using both of these methods, one cannot get the full local information about the above-mentioned properties. Impedance spectroscopy needs an exact model and can only distinguish between interfaces and therefore does not have local information for each interface. Nanoindentation, is destructive and does not provide any electrical information. One of the more effective tools used to overcome the problems encountered in electrical property measurement is Scanning Spreading Resistance Microscopy (SSRM). This technique simultaneously measures both electrical properties and topography. However, SSRM has some disadvantages such as rapid wearing of the tip, degradation of image resolution and low signal-to-noise ratio. These disadvantages stem from the high frictional force arising from continuous tip-sample contact during scanning. Recently, a new operational atomic force microscopy mode developed by Park Systems called PinPoint™ [10] AFM can be coupled with SSRM to offer scientists and engineers an innovative solution to avoid the troublesome frictional forces during a scan. This method operates in an approach-retract manner, ensuring a frictionless operation which eliminates the lateral force from continuous tip-sample contact. In addition, the integration of these methods with AFM enables it to acquire topography as well as electrical/mechanical property data simultaneously without changing the sample or tip. Here we demonstrate that PinPoint™ SSRM AFM effectively measures both electrical and mechanical properties of LIBs electrode surfaces at a much higher quality using a Park NX-Hivac atomic force microscopy system.

Experimental

An LIB electrode was investigated using a Park NX-Hivac AFM system [9]. The topographical, electrical and mechanical data of the sample were measured under high-vacuum to perform a 20 µm x 12 µm scan with a resolution of 256 x 150 pixels. Conducting this experiment under high-vacuum led to sensitivity and resolution improvements [9]. High-vacuum also led to accuracy and repeatability enhancements while minimizing damage suffered by the tip and/or sample. The force between the tip

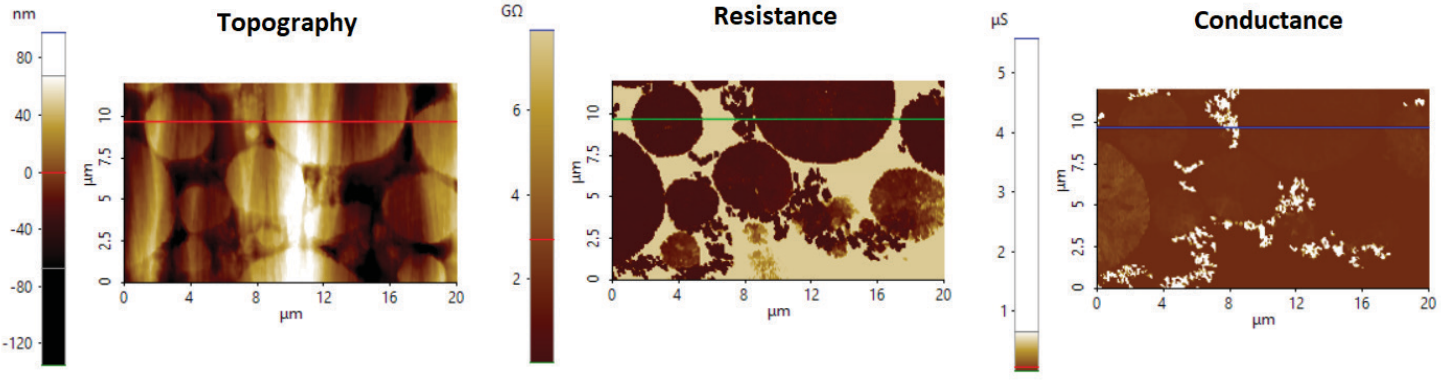

Figure 1. Topography (top-left) resistance (top-right) and conductance (middle-left) images acquired from an LIB electrode sample. Line profile (middle-right): Topography line profile (red line, y-axis on left), resistance line profile (green, y-axis on right), and conductance line profile (blue line, y-axis on right). 3D-overlay image of topography and conductance (bottom).

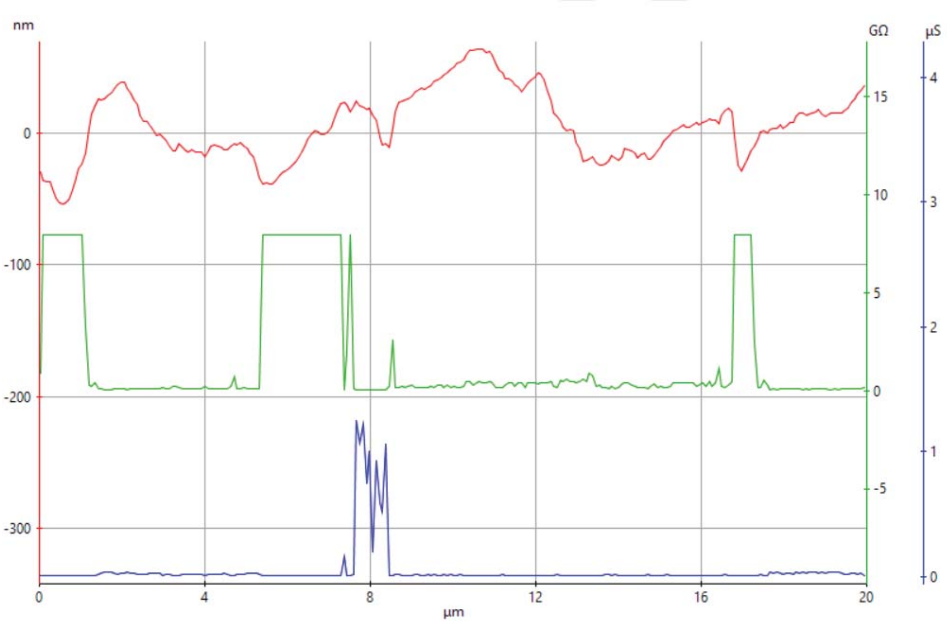

Line profile (above): Topography line profile (red line, y-axis on left) resistance line profile (green, y-axis on right), and conductance line profile (blue line, y-axis on right).

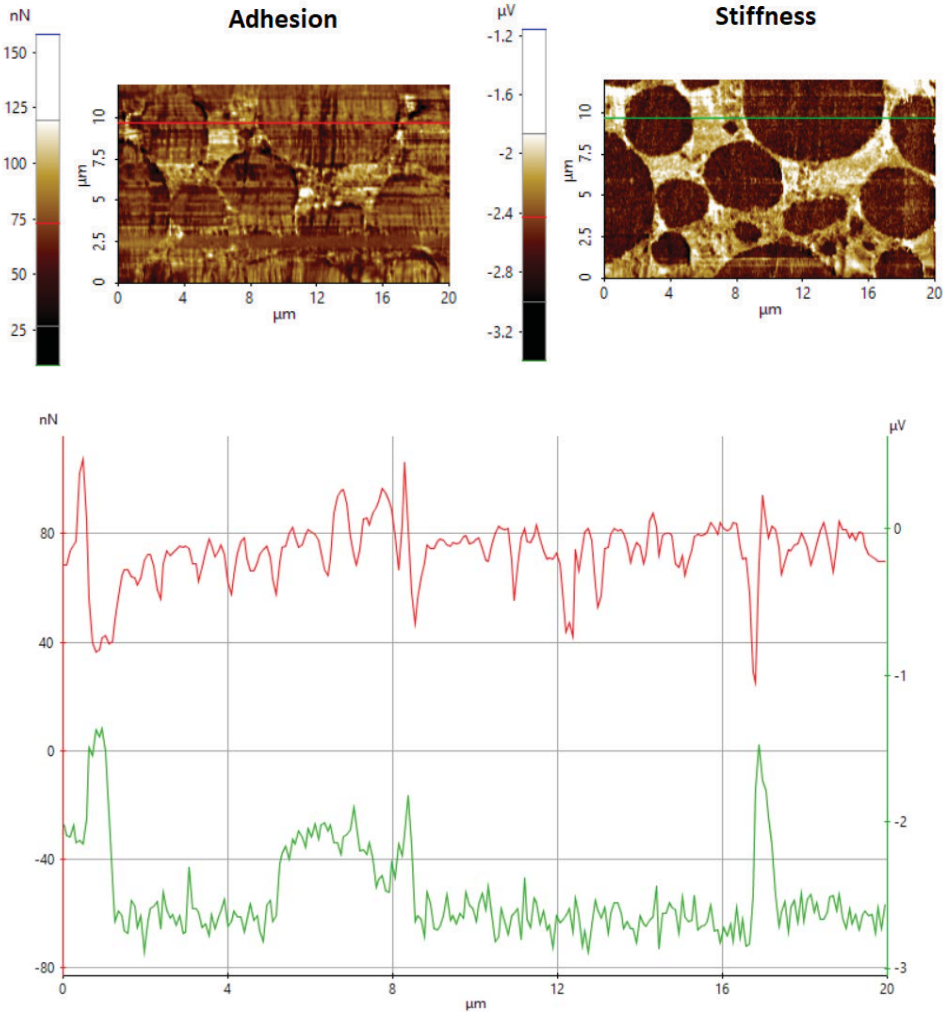

Figure 2. Adhesion (top-left) and stiffness image (top-right0 acquired from LIB electrode sample. Line profile (bottom): Adhesion line profile (red line, y-axis on left) and stiffness line profile (green, y-axis on right).

substantially lower than that conducted in ambient air or N_2, as the liquid film present under ambient conditions reduces the quality of the electrical contact[9]. A conductive diamond coated probe (NANOSENSORS™ CDT-NCHR) with a nominal force constant of 80 N/m was used in this experiment.

In Pinpoint™ SSRM, the sample's topography, electrical properties and mechanical properties can be acquired simultaneously. The conductive tip maps the topography by monitoring its feedback signal, approaching the sample until it reaches a predefined force threshold point, measuring Z scanner height and rapidly retracting. The current distribution of the samples is mapped each time the tip engages the sample surface. The current flow, produced by the applied bias voltage between the conductive tip and sample, is measured at each landing point to acquire the electrical data. Generally, the current flow is very small and needs to be augmented by a current amplifier before it can be processed into an image. The Park NX-Hivac is equipped with an internal current amplifier with a variable gain of 10^6~10^{12} V/A that is applicable to most measurements. The applied external sample bias used in this experiment was 3V. Additionally, at each point of the image, the force-distance curve is acquired and used to calculate the mechanical properties of the sample being measured. During data acquisition, the XY scanner stops and the contact time is controlled to give enough time for the scanner to acquire precise and accurate data.

Results and Discussion

The qualitative and quantitative results acquired during the experiment are shown in Figures 1 and 2. All images were analyzed using Park XEI image processing software developed by Park Systems; the software generated a corresponding line profile as well as image analysis. The Park XEI software maps the acquired signals into a color table. Figure 1 presents the topography and electrical data measured in the sample. The topography image (top-left) shows that the sample surface consists of circular shaped plateaus with diameters ranging from 2 µm to 8 µm. The circular plateaus with brighter colors represent areas with greater height while the areas with darker color represent low lying areas. The resistance image (top-right), feature brighter colored areas that represent higher surface resistivity while areas with darker colors represent lower surface resistivity. The darker colors on the conductance image (middle-left) represent areas with lower surface conductivity while brighter colors represent higher conductivity. By comparing the topography and resistance image, one can easily observed that circular plateaus with higher height have

lower resistance compared to low laying areas, while comparing the topography and conductance image will show that circular plateaus with higher height have higher conductance compared to low laying areas. This can also be observed in the 3D-overlay image of topography and conductance (bottom) acquired in Park XEI. Both resistance and conductance image also show a clear picture of the small grains surrounding the circular plateaus. It was observed that these small grains have lower resistivity and higher conductivity compared to the circular plateaus. Analysis of the corresponding line profile (bottom-right) of the topography, conductance and resistance images confirms that the circular plateaus are regions with highest height (approximately 50-60 nm). On the other hand, low lying areas possess highest resistivity (approximately 8 GΩ). The line profile of the conductance image shows that the tiny grains around the circular plateaus are regions with the highest conductivity (approximately 1.3 µS).

Figure 2 represents the mechanical data measured in the sample. In the stiffness images, the brighter areas represent a surface with higher stiffness and modulus while the darker areas correspond to the surface with lower stiffness and modulus. The adhesion image does not show significant variations between the plateaus. A tendency of higher adhesion is observed between the plateaus. The average adhesion force was measured to be 80 nN. The stiffness image shows noticeable stiffness variations in the sample surface. The measured stiffness value of the circular features represented by the dark color map is approximately –2.8 µV (note that the stiffness unit given here is for qualitative data comparative purposes and does not represent an absolute physical unit value of stiffness), while the areas represented by the bright color map were in a range from –1.5 to –2.0 µV.

Conclusion

A lithium ion battery electrode was successfully characterized by the Park NX-Hivac system using PinPoint™ SSRM. The data collected in this experiment demonstrate that this technique is an effective means for measuring the quantitative and qualitative topographical, electrical and mechanical data of advanced materials with improved image quality and data accuracy. Overall, the PinPoint™ technique described in this study will greatly help researchers and device engineers in understanding the electrical and mechanical behavior of certain materials with unique properties such as LIB electrodes.

References

[1] Tarasco M, et al., Issues and challenges facing rechargeable lithium batteries. Nature. 2001 Nov 15;414(6861):359-67.

[2] J. Chen, et al., Unveiling the Roles of Binder in the Mechanical Integrity of Electrodes or Lithium-Ion Batteries. Journal of The Electrochemical Society, 160 (9) A1502-A1509 2013).

[3] L. Vasconcelos, et al., Grid indentation analysis of mechanical properties of composite electrodes in Li-ion batteries. Extreme Mechanics Letters Volume 9, Part 3, December 2016, Pages 4.

[4] G. Kermani, et al., Review: Characterization and Modeling of the Mechanical Properties of Lithium-Ion Batteries. Received: 30 September 2017; Accepted: 24 October 2017; Published: 30 October 2017.

[5] A. Mishra, et al., Electrode materials for lithium-ion batteries. Materials Science for Energy Technologies Volume 1, Issue 2, December 2018, Pages 182-187.

[6] M. Park, et al., A review of conduction phenomena in Li-ion batteries. Journal of Power Sources, Received 12 May 2010 Received in revised form 16 June 2010 Accepted 17 June 2010.

[7] Y. Gao, et al., Mechanical reliability of alloy-based electrode materials for rechargeable Li-ion batteries. Journal of Mechanical Science and Technology 27 (5) (2013) 1205~1224.

[8] E. Reinholz, et al., Composition and Manufacturing Effects on Electrical Conductivity of Li/FeS2Thermal Battery Cathodes. doi: 10.1149/2.1191608jesJ. Electrochem. Soc. 2016 volume 163, issue 8, A1723-A1729

[9] Park Systems Introduces Park NX-Hivac, a High Vacuum SSRM AFM System for Optimal Results in Semiconductor Manufacturing Failure Analysis.

[10] J.Pineda, et al., Optimum Current Distribution Measurement of Zinc Oxide Nanorods via PinPoint™ Conductive AFM

[11] F. Susai, et al., Horizons for Li-Ion Batteries Relevant to Electro-Mobility: High-Specific-Energy Cathodes and Chemically Active Separators. doi: 10.1002/adma.201801348.

DESIGNING NANOSTRUCTURES BY NANOSPHERE MONOLAYERS AND DYNAMIC SHADOWING GROWTH

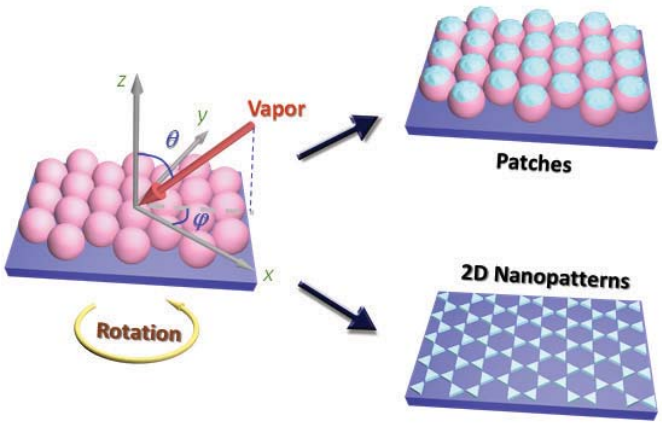

Figure 1. The general configuration of the nanosphere lithography and dynamic shadowing growth, and corresponding nanostructures that could be formed.

Yanfeng Wang, Yanjun Yang, and Yiping Zhao
Department of Physics and Astronomy, University of Georgia, Athens, GA 30602, USA

Introduction

Nanosphere lithography (NL) or natural lithography is a powerful but simple nanofabrication technique to produce arrays of nanostructures with hexagonal lattice arrangement.[1-4] Such a method was first reported by Fischer and Zingsheimin 1981 when they used a close-packed microsphere monolayer as a shadow mask to fabricate platinum disks.[5] When Van Duyne's group introduced this method for nanostructure fabrication in 1995,[2] it has then been widely investigated and evolved into one of the powerful nonconventional nanofabricationmethods.[6-9] In general, the NL process uses a close-packed nanosphere monolayer (NSML) as a shadow/etching mask, followed by multi-steps of deposition or etching or the combination of deposition and etching. Figure 1 illustrates the simplest situation for an NL process: a NSML is prepared on a flat substrate, and the substrate is used for vacuum deposition. After deposition, two kinds of nanostructures are formed: the deposited material could form patches on top of the nanospheres or smaller structures would be deposited directly onto the substrates through the voids between the nanospheres (we called these structures two-dimensional (2D) nanopatterns). The NSML could also be removed by different means so that only the 2D nanopatterns would be left on the substrates. Clearly, depending on the materials deposited or the final structures left on the substrates, the resulted nanostructures would have different physical or chemical properties. Since the nanospheres of various sizes can be purchased commercially,[10] and vacuum deposition and plasma etching systems are readily accessible by many labs in the world, the NL method becomes a simple, affordable, and very popular nanofabrication technique. In addition, the NL process is also a versatile technique to design different and complicated nanostructure if the deposition configuration or the NSML could be modified. For the deposition configuration as shown in Figure 1, the vapor incident angle θ (the angle between the vapor incident direction and the substrate surface normal) can be changed during the deposition so that the shadowing effect produced by the NSML could be varied. Also due to the periodicity and lattice symmetry of the hexagonal packed nanospheres, the deposition azimuthal angle ϕ (the angle between the projected vapor incident direction in x-y plane in Figure 1 with respect to one of the major axes of the hexagonal lattice (x-direction)) could also alter the shape of shadowing by the NSML. We broadly define the change of θ and ϕ in deposition configuration as dynamic shadowing growth (DSG). For example, Van Duyne's group has demonstrated the formation of elongated nanotriangle patterns by varying the θ angle during the deposition.[3] Kosiorek et al. has tuned both θ and ϕ to design variety of nanostructures.[11] In addition, by introducing etched NSMLs, complicated 2D nanopatterns can also be formed as demonstrated recently by Whitesides's group.[12] In fact, the change of the azimuthal angle ϕ would continuously produce different shapes of shadows, alter the location position and shape of the shadows; while the variation in the incident angle θ or the gap between the nanospheres could control the length and width of the shadows as well as their locations.

Here the versatility of the NL process by combining the NSMLs and DSG will be demonstrated. The morphologies of the resulting 2D nanostructures are characterized by an atomic force microscope (Park NX10) and their optical properties were obtained and related to the structural features.

Experiments

We use a home-made liquid-air interface method to assemble NSMLs as shown in Figure 2. In general, the creating of high quality NSMLs involved three steps, as shown in Figure 2a. The first step was to prepare well-dispersed nanosphere suspensions. The as-received polystyrene nanospheres were sonicated to ensure that they were well dispersed in liquid. Then the nanosphere suspension were "washed" several times by a centrifugation method. This washing procedure is necessary to remove surfactants that most companies put into the nanosphere suspension to stabilize the dispersion. The washing procedure was a critical step to improve the packing of the nanospheres during the formation of monolayers at the air-water interface. Then the suspension was dispersed/diluted in ethanol. The ethanol would help the nanospheres to quickly spread at the air-water interface. In Step 2, the cleaned nanosphere suspension was withdrawn into a syringe capped with a 20-gauge needle bent at a 90° angle towards a 15cm-diameter glass Petri dish partially filled with water. The Petri dish was carefully cleaned using a boiling piranha solution before used. The syringe was placed into a syringe pump and droplets of the nanosphere suspension were pumped into the water surface. When a droplet of the suspension landed onto the water surface, the ethanol lowered the local surface tension, causing the

water to flow radially away from the dropping location, and carrying the nanospheres to spread on the surface quickly. As more and more nanospheres floated on the water surface and began to form a monolayer,the ethanol induced surface flow of water also acted as a compression mechanism to push the nanospheres to stay closer to each other so that the surface packing density of the monolayer could be significantly improved. Figure 2b shows a photo of the experimental set-up and Figure 2c is a photo of the Petri dish when a monolayer of nanosphere film was formed on the air-water interface. After a large area monolayer film was formed, a Teflon ring was placed around the perimeter of the Petri dish to prevent the nanospheres from depositing on the side wall of the glassware. Then more water was pumped into the Petri dish to raise water level so that desired pieces of substrates were carefully slid below the monolayer film. In Step 3, water was pumped out from the Petri dish, and as the water level was lowered, the monolayer would be deposited onto the substrates as the water level was lower enough. Then the substrates were dried for an extended time period. Figure 2d shows a representative SEM image of a high quality NSML made in our lab. Here polysterene nanospheres (Polysciences Inc.) with a diameter of D = 500 nm were used.

Once the NSMLs were formed on the substrates, the size of the nanospheres could be reduced by reaction ion etching through a Trion Technology Phantom III RIE/ICP system. The etching was conducted at 40 mTorr with a 10 sccm oxygen flow, an inductively coupled plasma power of 25 W, and a reactive ion etch power of 10 W for different etching time duration t = 0, 50, 75, 150, 200, 300, and 400 s, respectively. Different Ag nanostructures were then fabricated using a custom-built electron beam deposition system. The chamber was pumped down to a base pressure of < 1×10^{-6} Torr. The deposition rate and total thickness of the films were monitored by a quartz crystal microbalance (QCM). Different NSML substrates etched at different time duration were loaded into the deposition chamber and Ag depositions were carried out at three different deposition configurations to show various simple 2D nanopatterns that could be formed: Strategy I: direct deposition of 60 nm (QCM thickness reading) Ag, *i.e.,* $\theta = 0°$. It is expected that the nanopatterns formed are the projected void patterns of NSMLs. Strategy II: to set $\theta = 53°$ and perform three consecutive depositions of 60 nm (QCM thickness reading) Ag at $\theta = 0°$, 120°, and 240°, respectively. The expected 2D nanopatterns should be three projected nanofeatures through the shadowing of the voids in NSMLs. Strategy III: to perform three consecutive depositions of 240 nm (QCM thickness reading) Ag at $\theta = 10°$ and $\phi = 0°$, $\theta = 20°$ and $\theta = 120°$, and $\phi = 30°$ and $\phi = 240°$, respectively. Since the projected shadow length is different at different θ angle, the resulting nanopatterns should possess handedness property. After the deposition, the samples were allowed to cool in vacuum before being removed from the chamber. Then the NSMLs were removed with the Scotch tape method. Any residual polysterene was washed away with toluene, and the samples were rinsed with acetone and then IPA before being dried under a N_2 gas flow. The resulted nanostructures formed on the surface of the substrates from various NSMLs and deposition configurations described above, were predicted by an in-house MATLAB program.[13] This program simulated the deposition process by projecting Ag vapor through the nanosphere monolayer mask at desired angles of θ and ϕ, but did not take into account of the shadowing effect of the thin film deposited on the PS nanospheres. Detailed information on this program can be found in Ref. 13. The morphologies of resulting samples were characterized by at atomic force microscope (Park NX10) and the corresponding optical properties were measured by a commercial UV–vis–NIR spectrophotometer (Jasco V-570) over a wavelength range of 400 nm to 2000 nm or by a home-built circular dichroism (CD) spectroscopic measurement system in a wavelength range of 400 nm to 1000 nm range.

Results and Discussion

Using AFM to characterize etched NSMLs

For the combined NSML and DSG method, it is very important to know the structure of the NSMLs, especially after plasma etching. Two methods could be used to characterize the etched NSMLs: direct imaging the etched monolayer or indirect measurement. For direct image method, one could take scanning electron micrographs (SEM) of the etched NSMLs and measure the size of the nanospheres as a function of the etching time. In most cases, the nanospheres we used are made by insulating materials, such as polystyrene or silica. Also, since we concern the optical property of the resulting structures, the NSMLs are prepared on glass substrates or other insulating substrates. Therefore, it is very hard to use SEM to obtain clear NSML images due to heavy charging effect. The other conventional imaging technique is AFM. As shown in Figures 3a and 3b, representative $D = 500$ nm NSMLs before etching and after etching ($t = 350$ s) are shown. If one directly compares these two images by naked eyes, they do not show much difference as the etched gap for $t = 350$ s sample is not large enough, and also there is the AFM tip convolution effect that could smoothen the sharp changes in height near two adjacent nanospheres. In order to obtain the etching effect, the height profiles of the spheres through their apparent centers were obtained and plotted as a function of the scanned position as shown in Figure 3c. In order to minimize the effect of AFM tip effect, we intentionally removed several data points near the sharp changes between two adjacent nanosphere. The height data can be fitted by a circle function, as shown by the solid curves in Figure 3c. From the fitting, one can obtainthe effective diameter D of the etched nanospheres. Such a method requires very careful data analysis. The indirect method

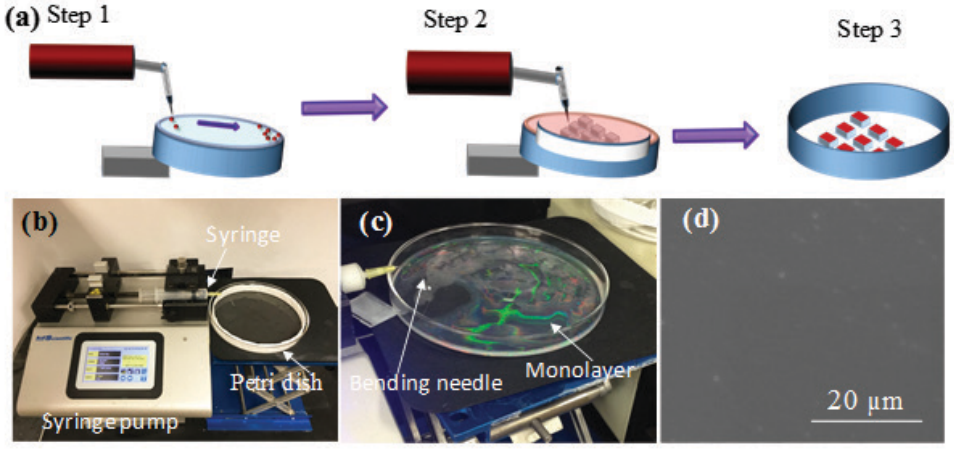

Figure 2 (a) Illustrations of the air-water interface method. (b) A photo of the home-made monolayer assembly system. (c) A photo showing nanosphere monolayer film floating on water surface in a glass Petri dish. (b) A representative SEM image of a high quality nanosphere monolayer on silicon substrate.

is to use the NSMLs as a shadow mask to directly deposit a layer of other materials at $\theta = 0°$ (Strategy I). After removing the NSMLs, one can use either the SEM or AFM to image the resulted structures, and one expects that inverted projected images of the NSMLs should be appeared. Here an unclaimed assumption was made, i.e., the resulting nanospheres still had a spherical shape, or the etching was isotropic. Figures 3d and 3e show the representative AFM images after the deposition of Ag by Strategy I for t = 200 and 400 s. We observe hexagonal patterned nanohole arrays with reduced nanohole diameter D when t increased. The hole diameter D was assumed to be the diameter of the etched nanospheres. Therefore, by plotting the D versus t, one could obtain the plasma etching performance for NSMLs (see Figure 3f). Based on our previous study,[14] the diameter of the etched nanosphere should follow the relationship, $D(t)=\sqrt{(D_0^2-(kt)^2}$, where D_0 is the initial diameter of the nanosphere while k is the etching rate. The red curve in Figure 3f shows the best fitting and we obtain k = 0.54± 0.02 nm/s.

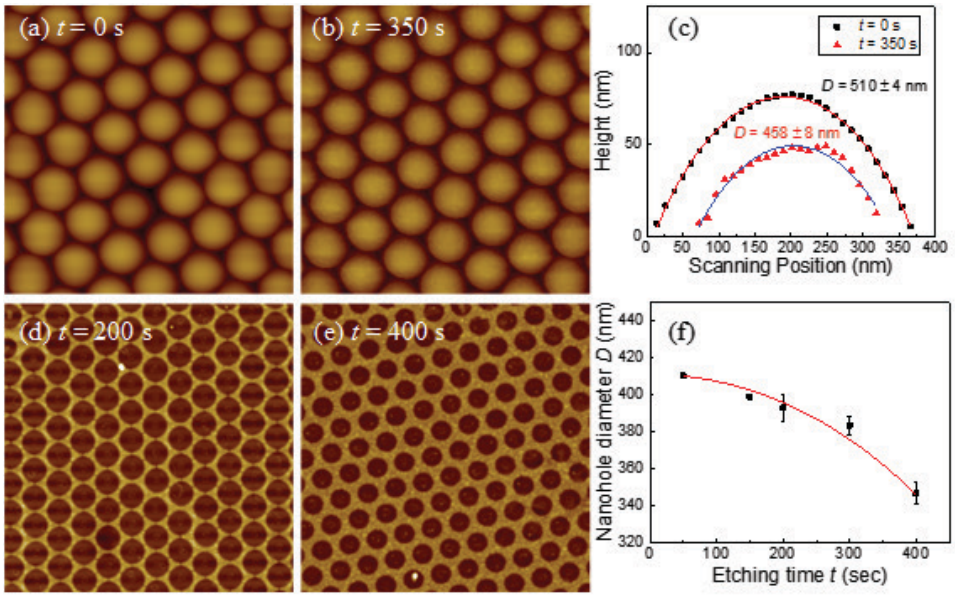

Figure 3 Representative AFM images of NSMLs for etching time t = (a) 0 s and (b) 350 s. The size of the images is 3 μm x 3 μm. (c) The height profiles of a single nanosphere before and after etching. The solid curves are the fitting results. Representative AFM images of Ag nanostructures deposited by Strategy I and after removing the nanospheres for t = (d) 200 s and (e) 300 s. The size of the images is 5 μm x 5 μm. (f) The plot of the hole diameter D from AFM images versus etching timet.

Morphology and optical properties of 2D nanopatterns by Strategy I

Figures 4a and 4b show the 2D patterns formed at small etching time for Strategy I, and the patterns formed for longer etching time are shown in Figures 3d and 3e. When the etching time t was small (Figure 4a), separated nanotriangle arrays in a hexagonal lattice were formed. When t increased to 150 s, adjacent nanotriangles started to connect together to form a 2D network (Figure 4b). When t increased further (t = 200 s, Figure 3d), a 2D nanohole network was formed, and the hole size became smaller when t increased to 400 s. Clearly, when t increased from 0 to 400s, the 2D patterns changed from discrete nanotriangle arrays to connected nanohole arrays, which are suggested from a shadowing deposition point of view since the gap between the nanospheres become larger when t increases. Thus, the optical properties of the 2D patterns are expected to have a transition from localized surface plasmon resonance (LSPR) to extraordinal optical transmission (surface plasmon propagation (SPP)).[15] Figure 4c shows the UV-Vis transmission spectra of the 2D patterns formed at different etching time. For small etching time t (≤ 100 s), there was a main dip at λ_c = 954 nm which corresponds to a strong dipole resonance. This is consistent with other studies on nanosphere lithography and nanotriangle arrays.[16-17] When t = 150 s and 200 s, the transmission spectra became very broad, and a dip could be extended beyond λ =1000 nm, which is due to the connection of

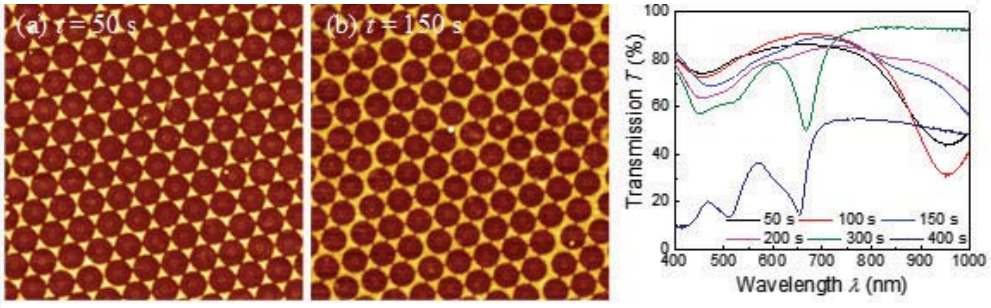

Figure 4Representative AFM images of 2D nanostructures for etching time t = (a) 50 s and (b) 150 s. The size of the images is 5 μm x 5 μm. (c) The UV-Vis transmission spectra of the samples deposited by Strategy I for various etching time t.

nanotriangles shown in Figure 4b or Figure 3d. The connections redshifted the trans mission dips. For t = 300 s and 400 s, a multi-dip and peak features were visible. Such a feature is due to a so-called extraordinary optical transmission (EOT) effect discovered by *Ebbesenet al.* due to the nanohole network.[18] The dip around λ = 650 nm is the Woods anomaly position while the broad transmission peak around λ = 700 nm is the EOT peak due to plasmon-grating coupling.[19] Clearly, as the etching time increases, the morphology changes from disconnected nanotriangles to connected triangles, then to the nanohole network, and the optical response varies from LSPR to EOT.

Morphology and optical properties of 2D nanopatterns by Strategy II

Figures 5a- 5c show some representative AFM images of the 2D patterns formed at etching time t = 200, 300, and 400 s for Strategy II. Since this strategy involves three different depositions, the patterns become more complicated but they can also be predicted by our in-house MATLAB program. The predicted structures are also shown in Figure 5. For t < 200 s, no 2D patterns were observed on the surface due to large vapor incident angle ($\theta = 53°$) and small gaps between nanospheres. For t = 200 s, clusters of nanobars were formed (Figure 5a). Each cluster consisted of three nanobars, each bar had a 120° angle with respect to adjacent bars, which is consistent with the deposition strategy. In the MATLAB prediction, the lengths of the three bars were the same; while from the AFM image, the lengths of the bars were 250±10 nm, 170±10nm, 170±10nm, and corresponding widths were 90±5nm, 99±4nm, and 98±5nm, respectively. The slight difference in the bar lengths was due to the extra shadowing effect induced

by films deposited onto the nanosphere surfaces. For ***t*** = 300 s, two characteristic hole shapes could be formed according to the simulation: small triangular nanoholes and large irregular hexagonal holes (Figure 5b). The large hexagonal hole was the overlap of two large triangular holes with about 90o orientation difference. The AFM image shows almost the same pattern. Compared to Figure 5a, there were more Ag coverages in Figure 5b. For *t* = 400 s, also a complex hole pattern with two characteristic hole features was expected: one was a large triangle hole, and other was a windmill shaped hole (Figure 5b). The AFM image showed the exactly predicted features. In this case, the Ag had more coverage on the surface. For all the three samples measured by AFM, the thickness of the patterns were a constant, about 15 ±1nm. The optical transmission spectra $T(\lambda)$ of the corresponding samples are shown in Figure 5d. For the *t* = 50 and 75 s samples, there was almost no spectral features presented in $T(\lambda)$ and the $T(\lambda)$ values of the entire wavelength range were close to 100%, which indicates that there were no nanostructures deposited on the substrate. However, for the *t* = 200 s sample, there was a sharp dip occurred at λ_c = 454 nm, which is the LSPR wavelength due to the nanobar clusters. For the *t* = 300 s sample, a larger dip occurred at λ_c = 460 nm; and for the *t* = 400 s sample, the resonance dip redshifted to λ_c = 500 nm. Clearly when *t* increased, the dip value became smaller, which reflects a high absorbance. This is due to the factor that the Ag coverage on the surface became larger and larger with the increase of *t*.

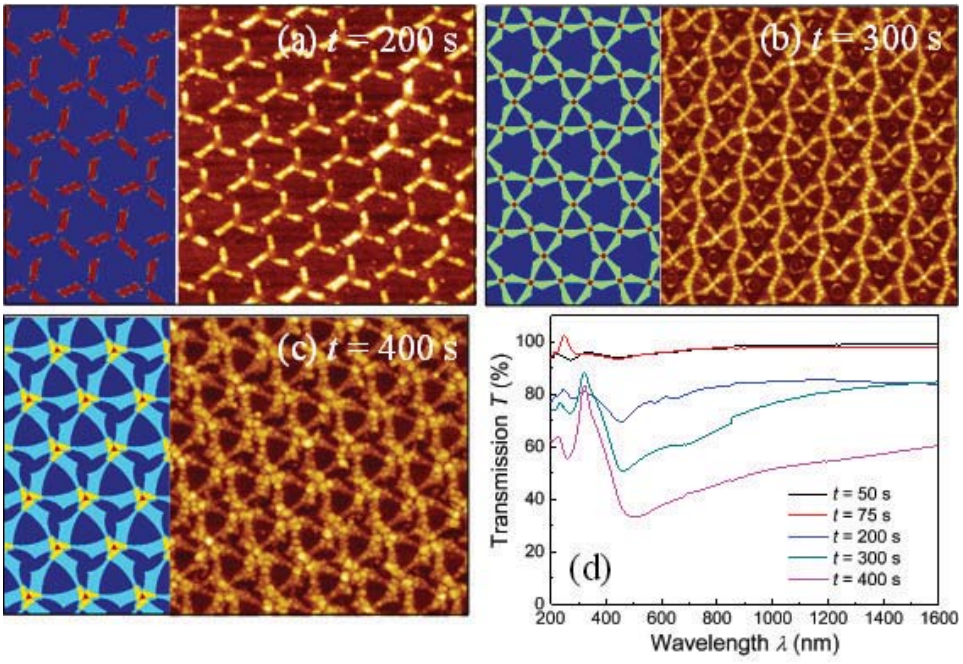

Figure 5 Representative AFM images of nanostructures deposited by Strategy II for etching time t = (a) 200 s, (b) 300 s, and (c) 400 s, respectively. The size of the images is 3 μm x 3 μm. The left panel of each AFM image shows the simulation result by our in-house MATLAB program. (d) The UV-Vis transmission spectra of the samples deposited by Strategy II for various etching time t.

Morphology and optical properties of 2D nanopatterns by Strategy III

Figures 6a - 6c show some representative AFM images of the 2D patterns formed at etching time *t* = 200, 300, and 400 s for Strategy III. Since this strategy involves three different depositions at different 0 angle, the shadowing length due to the nanospheres would be different in three azimuthal directions, which means the symmetry of the pattern would be broken, and the resulting structures should show certain handedness property, i.e., chirality. Figure 6a shows the patterns for *t* = 50 s sample, with disconnected double triangle clusters. For the *t* = 200 s sample (Figure 6b), larger connected triangular-shaped clusters were visible, and near each cluster, there was a small nanoparticle available. For *t* = 300 s sample (Figure 6c), honeycomb like networks were formed. Unlike the jointed triangular structures in Figure 4b or the nanohole networks shown in Figure 3d, the deposited Ag had an uneven distribution along the skeleton of the honeycombs. The joint of three adjacent arms (height ~ 145 nm) has a larger height than that (~ 80 nm) of the arms. Figure 6d shows the corresponding optical transmission spectra $T(\lambda)$ of these samples. For the *t* = 50 sample, there was a transmission dip occurred at λ_c = 747 nm, which corresponded to the LSPR resonance of the disconnected double triangle features. When t increased to 100 s, the dip redshifted to λ_c = 767 nm, which means the structures

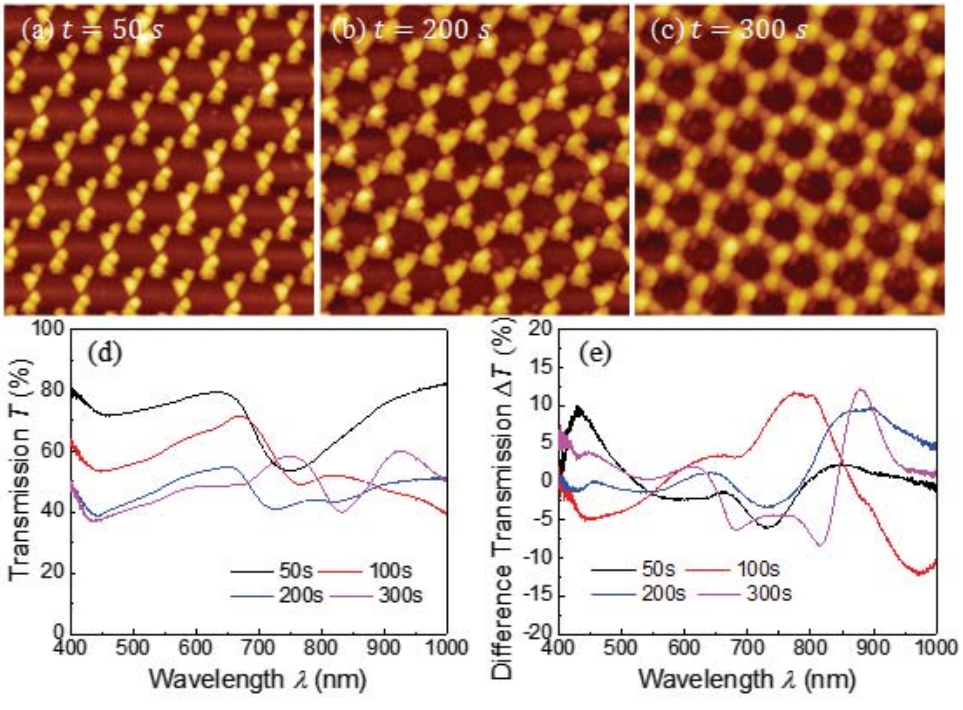

Figure 6 Representative AFM images of nanostructures deposited by Strategy III for etching time *t* = (a) 50 s, (b) 200 s, and (c) 300 s. The size of the images is 3 μm x 3 μm.
(d) The UV-Vis transmission and (e) The circular dichroism spectra of the samples deposited by Strategy III for various etching time *t*.

For the t = 200 s sample, the transmission over the entire spectrum became significant lower and there was a broad dip between λ = 650 to 850 nm. For the t = 300 s sample, an EOT type of response was obtained, with a dip at λ =832 nm and an EOT peak at λ = 926 nm. Since the resulted structures were expected to have handedness, which infers that when a right-hand or left-hand circularly polarized (RCP or LCP) light interacts with the structures, the response would be different. The difference between the transmission spectra of the LCP and RCP, $\Delta T(\lambda)$, called circular dichroism (CD) spectrum, should not be zero. Figure 6e shows the CD spectra of the corresponding samples. All the samples show non-zero CD spectra. For the t = 50 sample, a dip in $\Delta T(\lambda)$ occurred at λ = 732 nm, which is very close to the LSPR dip at λ_c = 747 nm. For the t = 100 s sample, a huge positive peak occurred at λ = 785 nm and a corresponding dip occurred at λ = 973 nm. For the t = 200 s sample, a broad peak appeared at λ = 877 nm. A sharp peak also was observed at the same location for the t = 300 s sample. Clearly all the samples demonstrated the CD response.

Conclusions

In summary, we have demonstrated that when combining NSMLs and DSG, various nanostructures can be designed and fabricated. The resulted nanostructures can be constructed by adjusting two sets of important parameters, the deposition configuration parameters, i.e., the vapor incident angle θ and the azimuthal angle φ; and the configuration of NSMLs, i.e., the gaps between the adjacent nanospheres. Also geometrically complicated nanopatterns could be designed by tuning the way to perform the deposition, for example, using multi-step deposition. AFM is a powerful technique to characterize the morphology of the resulting nanostructures and these nanostructures demonstrate different plasmonic properties and are expecting to have different applications.

Acknowledgments

This work is supported by the National Science Foundation under Grant ECCS-1609815 and ECCS-1808271.

References

[1] Deckman, H.; Dunsmuir, J., Natural lithography. Applied Physics Letters 1982,41 (4), 377-379.
[2] Hulteen, J. C.; Van Duyne, R. P., Nanosphere Lithography - a Materials General Fabrication Process for Periodic Particle Array Surfaces. J Vac Sci Technol A 1995,13 (3), 1553-1558.
[3] Hulteen, J. C.; Treichel, D. A.; Smith, M. T.; Duval, M. L.; Jensen, T. R.; Van Duyne, R. P., Nanosphere lithography: Size-tunable silver nanoparticle and surface cluster arrays. J Phys Chem B 1999,103 (19), 3854-3863.
[4] Zhang, G.; Wang, D. Y., Colloidal Lithography-The Art of Nanochemical Patterning. Chemistry-an Asian Journal 2009,4 (2), 236-245.
[5] Fischer, U. C.; Zingsheim, H., Submicroscopic pattern replication with visible light. Journal of Vacuum Science and Technology 1981,19 (4), 881-885.
[6] Zhang, J. H.; Li, Y. F.; Zhang, X. M.; Yang, B., Colloidal Self-Assembly Meets Nanofabrication: From Two-Dimensional Colloidal Crystals to Nanostructure Arrays. Advanced Materials 2010,22 (38), 4249-4269.
[7] Li, Y.; Duan, G. T.; Liu, G. Q.; Cai, W. P., Physical processes-aided periodic micro/nanostructured arrays by colloidal template technique: fabrication and applications. Chemical Society Reviews 2013,42 (8), 3614-3627.
[8] Ye, X. Z.; Qi, L. M., Two-dimensionally patterned nanostructures based on monolayer colloidal crystals: Controllable fabrication, assembly, and applications. Nano Today 2011,6 (6), 608-631.
[9] Yang, S. K.; Lei, Y., Recent progress on surface pattern fabrications based on monolayer colloidal crystal templates and related applications. Nanoscale 2011,3 (7), 2768-2782.
[10] Zhang, G.; Wang, D., Colloidal lithography—the art of nanochemical patterning. Chemistry–An Asian Journal 2009,4 (2), 236-245.
[11] Kosiorek, A.; Kandulski, W.; Chudzinski, P.; Kempa, K.; Giersig, M., Shadow nanosphere lithography: Simulation and experiment. Nano Lett 2004,4 (7), 1359-1363.
[12] Nemiroski, A.; Gonidec, M.; Fox, J. M.; Jean-Remy, P.; Turnage, E.; Whitesides, G. M., Engineering Shadows to Fabricate Optical Metasurfaces. Acs Nano 2014,8 (11), 11061-11070.
[13] Larsen, G. K.; He, Y.; Ingram, W.; Zhao, Y., Hidden chirality in superficially racemic patchy silver films. Nano Lett 2013,13 (12), 6228-32.
[14] INGRAM, W. THE FABRICATION AND APPLICATION OF PLASMONIC NANOPATTERNS BY SHADOW NANOSPHERE LITHOGRAPHY. The University of Georgia, Athens, GA, 2016.
[15] García de Abajo, F. J., Colloquium: Light scattering by particle and hole arrays. Reviews of Modern Physics 2007,79 (4), 1267-1290.
[16] Jensen, T. R.; Schatz, G. C.; Van Duyne, R. P., Nanosphere Lithography: Surface Plasmon Resonance Spectrum of a Periodic Array of Silver Nanoparticles by Ultraviolet−Visible Extinction Spectroscopy and Electrodynamic Modeling. The Journal of Physical Chemistry B 1999,103 (13), 2394-2401.
17. Whitney, I.; Yizhuo, H.; Keenan, S.; William, M. D.; Dexian, Y.; Yiping, Z., Tuning the plasmonic properties of silver nanopatterns fabricated by shadow nanosphere lithography. Nanotechnology 2016,27 (38), 385301.
18. Ebbesen, T. W.; Lezec, H. J.; Ghaemi, H. F.; Thio, T.; Wolff, P. A., Extraordinary optical transmission through sub-wavelength hole arrays. Nature 1998,391, 667.
19. Li, Y., Plasmonic optics: theory and applications. SPIE Press: 2017.

Dr. Yiping Zhao received his B.S. degree in Electronics from Peking University in 1991, and MS degree in condensed matter physics from Institute of Semiconductors, Chinese Academy of Sciences in 1994. He obtained his Ph.D. degree in Physics at Rensselaer Polytechnic Institute in 1999. He is currently a Distinguished Research Professor at the Department of Physics and Astronomy in University of Georgia, a fellow of the International Society of Optics and Photonics (SPIE) and American Vacuum Society (AVS). Prof. Zhao is the author or co-author of more than 280 peer reviewed journal papers, 2 books, 7 book chapters, and 12 US patents. His major research interests are nanostructures and thin films fabrication and characterization, plasmonic nanostructures, chemical and biological sensors, nano-photocatalysts, and nanomotors.

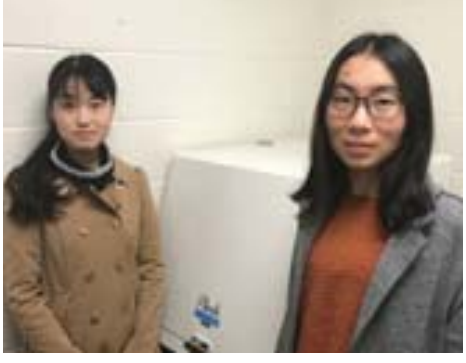

Yanfeng Wang (Left) is a PhD student from Tsinghua University and is now in a joint program under the supervision of Prof. Yiping Zhao in University of Georgia. Her current research focuses on the nanostructures fabrication and characterization, plasmonic nanostructures.

Yanjun Yang (right) is a PhD student at the University of Georgia under the supervision of Prof. Yiping Zhao. Her current research focuses on the fabrication, characterization and application of plasmonic nanomaterials for SERS/SPR based biochemical sensing and detections.

CEINT Center for the Environmental Implications of NanoTechnology

NANOTECHNOLOGY AND THE ENVIRONMENT: HOW THE IMPLICATIONS OF NANO PARTICLES ARE STUDIED AT THE CENTER FOR ENVIRONMENT IMPLICATIONS OF NANOTECHNOLOGY

Duke Green Lab Gold — A Duke University Green Lab

Duke University is home to several of the world's top environmental programs and is headquarters for the Center for the Environmental Implications of NanoTechnology (CEINT).CEINT is a collaborative effort bringing together researchers from Duke, Carnegie Mellon University, Howard University, Virginia Tech, University of Kentucky, Stanford University, and Baylor.

Duke does fundamental research in environmental engineering focusing on technologies at the energy and environment interface including environmental nanotechnology, membrane science, water treatment, desalination and water reuse, particle transport and surface chemistry in natural and engineered environments.

Photo: Founder and Director of CEINT, Mark Weisner was the eighteenth recipient of the NWRI Athalie Richardson Irvine Clarke Prize for excellence in water research in 2011. The Clarke Prize is awarded annually to an outstanding individual residing in the U.S. who has implemented exceptional water science research/ and or policy development to solve real-world water challenges, recognized by the International Congress of Distinguished Awards as one of the most prestigious awards in the world. His work in developing nanomaterial-based technologies for water treatment led him to consider the possible detrimental effects that these materials might have on human health and the environment – in effect, pioneering the field of environmental implications of nanotechnology.

An Interview with Mark Wisner, Director, Center for Environment Implications of NanoTechnology

The Center for the Environmental Implications of NanoTechnology (CEINT) was created in 2008 with funding from the National Science Foundation and the US Environmental Protection Agency, and performs fundamental research on the behavior of nano-scale materials in laboratory and complex ecosystems. The center was funded by $30 million in grants from the National Science Foundation and the US Environmental Protection Agency (US EPA) over the course of 10 years, and in that decade CEINT published a vast body of work explaining the environmental fate of nanomaterials, and organism and ecosystem responses to exposures to those materials. Research includes all aspects of nanomaterial transport, fate and exposure, as well as ecotoxicological and ecosystem impacts. Additionally, CEINT is developing risk assessment tools to provide guidance in assessing existing and future concerns surrounding the environmental implications of nanomaterials.

CEINT was launched by Duke Professor of civil and environmental engineering and principal investigator Mark Wiesner when the boom in nanotechnology was flooding the markets with nanoparticles in everything from additives to sensors and electronics.

The new center consisting of collaborators from Duke, Carnegie Mellon, Howard University, Virginia Tech, Stanford University, the University of Kentucky and Baylor University, with highly advanced nanoengineering programs began exploring fundamental questions about the fate of nanomaterials in the environment, and the implications of their presence. Their unique approach uses outdoor experimental facilities where water, soil, flora and fauna approximate real freshwater wetland ecosystems.

"GENERALLY, THE IMPACT OF NANOTECHNOLOGY ON THE ENVIRONMENT HAS BEEN EXTRAORDINARILY POSITIVE. NANO HAS ENABLED NEW TECHNOLOGIES FOR MEASUREMENT OF CONTAMINANTS IN THE ENVIRONMENT, IMPROVED WATER AND AIR QUALITY MANAGEMENT TECHNOLOGIES, REDUCED ENERGY USAGE THROUGH MORE EFFICIENT LIGHTING TECHNOLOGIES, BETTER ENERGY STORAGE, SOLAR ENERGY TECHNOLOGIES AND MUCH MORE."

"OUR CONCLUSION IS THAT THE BENEFITS OF MANUFACTURED NANOMATERIALS OUTWEIGH THE RISKS, BUT AT ITS HEART, THE RESEARCH PROBLEM IS ONE OF FATE AND TRANSPORT—AND EVERY RAY OF LIGHT THAT CEINT HAS SHONE ON THE APPLICATIONS, INTERACTIONS, AND IMPLICATIONS OF NANOMATERIALS IS HELPING TO SOLVE IT."

Photo: Dr. Mark Weisner, Director of CEINT has made many important contributions on the potential for nanoparticles to accumulate in the environment.

"Nothing is more important than the careful stewardship and development of our water resources" - Mrs. Athalie Richardson Irvine Clarke (The Clarke Prize Founder)

"Our conclusion is that the benefits of manufactured nanomaterials outweigh the risks," said Dr. Weisner, Director of CEINT and coauthor of Environmental Nanotechnology: Applications & Impacts of Nanomaterial. "Considering the life cycle effects of nanoproduction, we have determined that the risks are relatively small using nano particles that are made from particles we know are safe."

The goal of the CEINT research is to predict where certain nanomaterials will go in the environment, how long they will stay there and what effect they will have long term. "We have overestimated the risk of nanoparticles in the environment," adds Wiesner, who is also a professor of civil and environmental engineering at Duke. "The role of nanomaterial research is to protect public health and the environment and have the right technologies making their way into the markets. Understanding the actual effect of nanomaterials in the environment will help us make decisions about whether or not to use certain ones."

While we cannot see nanoparticles with the naked eye, investigating their impact on living things and developing tools to assess current and future risk at the Center for Environmental Implications of Nanotechnology tells us how these materials end up in the environment—and what they do once they get there.

"The development of nanometrology tools has had an enormous impact on NanoEnvironmental Engineering", states Dr. Weisner. "Microscopes of today have changed everything because we can image particles of different shapes and sizes, these new tools in microscopy have allowed us to examine exactly what filtered particles are."

In the new age of nanometrology, images at the nanoscale open new horizons for researchers like the ones entering the CEINT program. "We can begin to characterize the NanoScience world in a way that was not possible 30 years ago," adds Weisner.

"NANOTECHNOLOGY IS PERHAPS THE FIRST EXAMPLE OF A NEW GROUP OF TECHNOLOGIES THAT HAS BEEN EVALUATED EARLY IN ITS DEVELOPMENT AND COMMERCIALIZATION TRAJECTORY RATHER THAN WAITING FOR ENVIRONMENTAL PROBLEMS TO ARISE. WHILE THERE WILL ALWAYS BE IMPACTS OF ANY HUMAN ACTIVITY ON THE ENVIRONMENT, THE FIELD OVERALL HAS BEEN PROACTIVE IN MINIMIZING THE POSSIBILITY AND THE MAGNITUDE OF SUCH IMPACTS."

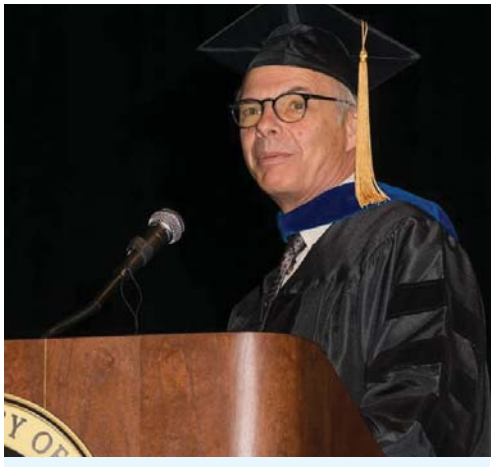

Photo: Alumnus Mark Wiesner delivers the keynote speech to December 2017 graduates of the UI College of Engineering where he encouraged engineering graduates to "be scientific, be ethical, and be creative," and told them to prepare for the future, because "the torch (of technology and science) is being passed to you."

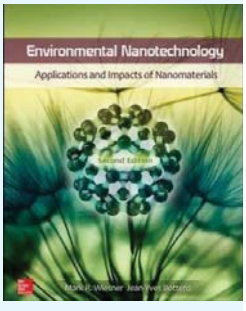

Photo: Now in the 2nd edition, Environmental Nanotechnology co edited by Mark R. Weisner and Jean-Rves Bottero and co written by a team of leading experts from around the world provides a through look at nanomaterial technologies, their use in engineering applications, and their impact on the environment.

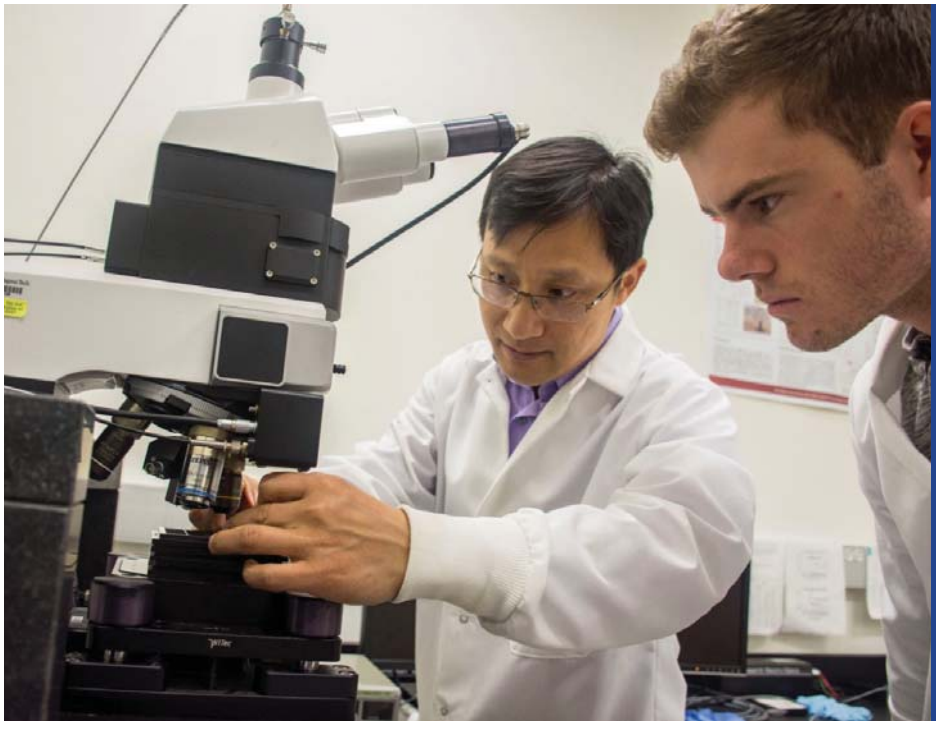

PARTICLE RESEARCH USING AFM AT VIRGINIA TECH'S NANO EARTH LAB, WEINAN LENG, VIRGINIA TECH SUSTAINABLE NANO TECHNOLOGY LAB MANAGER & RESEARCH SCIENTIST IN CIVIL AND ENVIRONMENTAL ENGINEERING

Pictured above, Dr. Weinan Leng, who researches Nanoparticle-based sensors for environmental applications and Laser-based techniques (Raman and surface enhanced Raman scattering) for nanoparticle tracking.

AT VIRGINIA TECH, ONE OF THE MEMBERS OF CEINT THE THE VIRGINIA TECH CENTER FOR SUSTAINABLE NANOTECHNOLOGY (VTSUN), IS FOR STUDENTS AND POSTDOCS WHO ARE RESEARCHING ENVIRONMENTAL NANOSCIENCE AND TECHNOLOGY FROM DIFFERENT PERSPECTIVES AND IS EQUIPPED WITH A RANGE OF STATE-OF-THE ART NANOMETROLODGY TOOLS INCLUDING ATOMIC FORCE MICROSCOPE, TEM AND SEM.

AN INTERVIEW WITH DR. WEINAN LENG, LABORATORY DIRECTOR OF VIRGINIA TECH NATIONAL CENTER FOR EARTH AND ENVIRONMENTAL NANOTECHNOLOGY INFRASTRUCTURE (NANOEARTH)

How do you use Atomic Force Microscopes in your research?
In most of cases, I utilize AFM for topographic measurements, such as particle size, surface roughness.

What features of Atomic Force Microscope are most useful and why?
The most useful feature of AFM is to measure incredible small particles with a high degree of accuracy.

Can you show an example of silver nano particle imaging and explain why these images were taken and what they tell us?
Figure 1. AFM images of uncoated and coated AgNPs measured after 1 and 14-days dissolution. The left panel is the AFM image for the original AgNPs without coating and dissolution; on the right side (labeled a-h) are the AFM images for uncoated and coated AgNPs after 1 and 14 days. (Liu, C., Leng, W., Vikesland, P. J., Controlled Evaluation of the Impacts of Surface Coating on Silver Nanoparticle Dissolution Rates, ES&T, 2018, 52[(5)],2726-2734.)

This is an example of how to utilize a highly sensitive AFM to examine engineered nanomaterial dissolution, which is one of NSF projects that has been done in the group of Prof. Peter Vikesland at Virginia Tech. The AFM images in Figure 1illustrate how surface coatings affect silver nanoparticle dissolution rates. In this research, arrays of surface adhered silver nanoparticles were produced via nanosphere lithography, and AFM provides a convenient technique to measure changes in particle height which is related to the kinetics of AgNP dissolution.

Figure 1

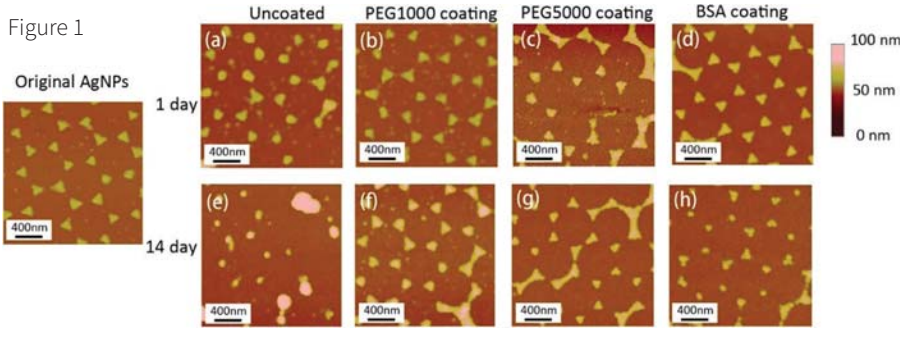

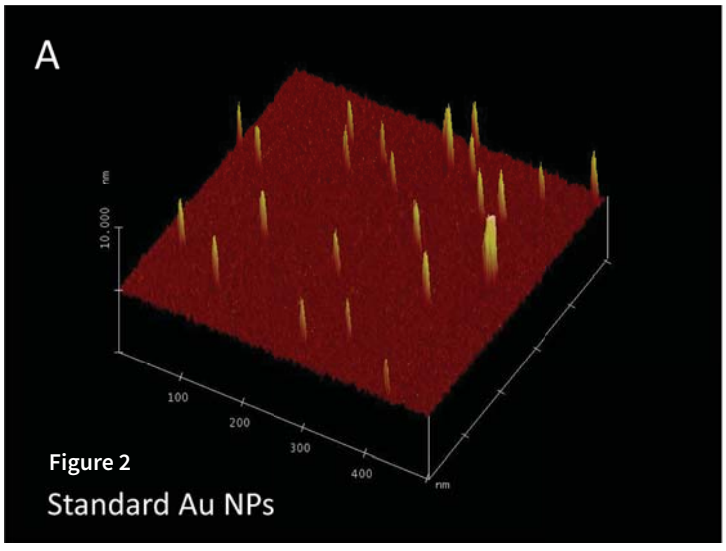

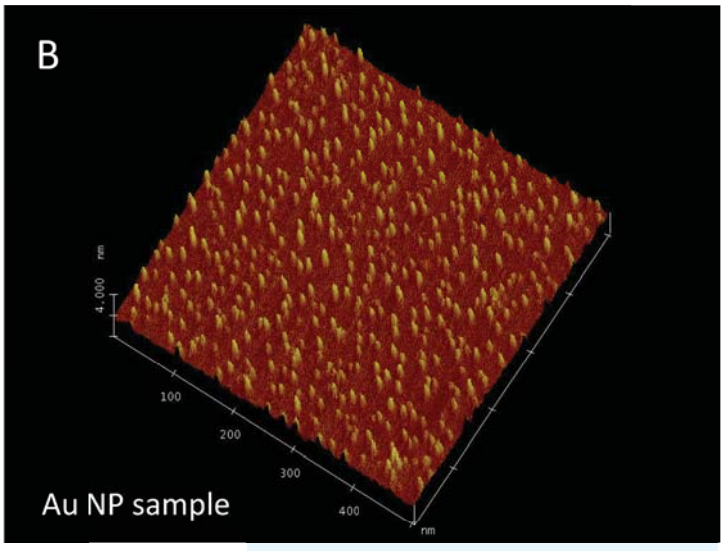

Figure 2

Can you show an example of gold nano particle imaging and explain why the images were taken and what they tell us?

In Figure 2, on the next page, AFM images of 5nm gold nano particle (Au NP) standard (A) and 1 nm gold hydrogel sample (B).

This is one of the most attractive applications of AFM which provides a quick survey for very small particles (less than 5 nm) in a low concentration that are not created as an artifact of the electron beam in an electron microscope. The standard image shows how accuracy of height measurements which can reflect particle size.

How do you think the imaging of NanoParticles can help us with the environmental issues we are facing?

Following the example in question 3, once a well-controlled nano structure was designed and modelled for the engineered nano materials, which can be avoidthe severe limitations of many alternative methodologies, such as the aggregation using realistic nanoparticle solution.

Findings based on AFM imaging will aid efforts to engineer environmentally benign nanomaterials and to predict their environmental impacts.

What do you like best about working in the NanoEarth group at VaTech?

I love being an instrument specialist, and being asked for my participation in a lot of cool projects of NanoEarth users. Every technical service, data report and critical observation you give will have your fingerprint on it in a good way. It gives me great job satisfaction that significantly outweighs the stress, the time and the hard work.

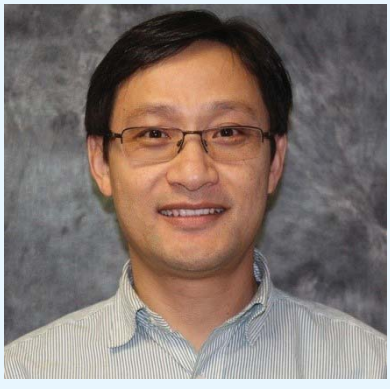

Dr. Weinan Leng is a Laboratory Director of Virginia Tech National Center for Earth and Environmental Nanotechnology Infrastructure (NanoEarth), operating Raman-AFM microscope, X-ray photonelectron spectroscope, multimode AFM, BET, UV-vis-NIR spectrometer and DLS instrument. He received his PhD from Southeast University of China in Biomedical Engineering for his work on the fabrication and characterization of second-order nonlinear optical polymers and their application in electro-optical devices.

He moved to the United States as a post-doctoral researcher in the group of Prof. Anne Myers Kelly (University of California, Merced) working on the development of laser optical spectroscopes. From 2009 to 2018, Dr Leng was a Research Scientist at Virginia Tech, where he implements his research lines originated in Environmental Nanotechnology.

Since September 2018, Dr Leng is a senior Research Associate at the Institute for Critical Technology and Applied Science of Virginia Tech.

APPLICATION NOTE

MECHANICAL PROPERTIES OF LIVE AND FIXED CELLS MEASURED BY ATOMIC FORCE MICROSCOPY AND SCANNING ION CONDUCTANCE MICROSCOPY

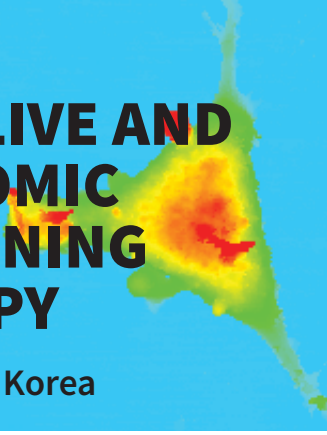

Jake Kim, Moses Lee and Cathy Lee, Park Systems Corp., Suwon, Korea

Abstract

During the process of cell sample preservation, cell fixation plays an essential role for a wide range of biological assays. To determine the importance of this procedure, a comparative analysis was performed between live and fixed cells using Scanning Probe Microscopy (SPM) techniques such as Atomic Force Microscopy (AFM) and Scanning Ion Conductance Microscopy (SICM) for mechanical property measurements and surface fluctuation measurements, respectively. Results from these techniques provide a broad understanding of how cell fixation affects the mechanical properties of cells, and offer new opportunities for the establishment of cell fixation protocols.

Introduction

One of the primary objectives of cell fixation for in-vitro studies is preservation of the cell or cellular components in a life-like state by conserving essential chemical and physical characteristics of the cells. Cell fixation is also useful in immunostaining by allowing antibodies to access intracellular structures [1]. Comparing live and fixed cells, the fixed cell maintains a more uniform architecture over the entire cell surface [2]. However, there is no systematic assessment or correlation between changes in mechanical properties of live and fixed cells. By observing various states of cell fixation and the living cells, there is an opportunity to optimize cell fixation protocols, and gain valuable knowledge in aiding the process of cell fixation. Many fixation agents are available for cross-linking cell membranes and cytoplasmic proteins, with paraformaldehyde (PFA) as the most widely used for cell and tissue samples [1-3]. PFA works by covalently cross-linking molecules, bonding them together and creating an insoluble meshwork that alters the mechanical properties of the cell surface. In order to investigate the mechanical properties of live and fixed cell structures fixed with PFA, Atomic Force Microscopy (AFM) and Scanning Ion Conductance Microscopy (SICM) were used to measure the elastic modulus and surface fluctuation, respectively [3-6].

Experimental set-up

Cell sample

The cell sample used consisted of mouse fibroblast L929 cells (ATCC, USA) cultured in Dulbecco's modified eagle medium (DMEM; Invitrogen Life Technique, USA) complemented with 10% fetal bovine serum (Thermo Fisher Scientific, US) together with 1% penicillin/streptomycin (Invitrogen Life Technique, USA) at 37°C in a humidified atmosphere with a 5% CO_2 concentration. Cells (with densities of 1x104 / mL) were placed on a 35 mm diameter cell culture petri dish (NUNC, Denmark),washed three times with phosphate buffered saline (PBS, Sigma-Aldrich, US) and treated with a 4% PFA solution for 5 min. The fixed cell samples were rinsed with PBS three times prior to conducting AFM and SICM experiments.

Set-up of AFM and SICM

The setup for cell imaging consisted of the Park Systems scanning probe microscope (Park NX-Bio, Park Systems, Korea) equipped with an inverted optical microscope (Nikon Corp., Japan) specifically designed for biological applications. The AFM can gather the mechanical properties of a sample as well as cell surface information of soft material samples using SICM. All experiments performed on live cells were carried out in a live cell chamber. The chamber conditions of the live cell were regulated to 37 °C, 5% CO_2 and 95% humidity and had the necessary environment to sustain living cell cultures.

AFM measurements for Young's modulus of cells

The AFM was used to obtain force curve measurements to estimate the Young's modulus of cells. A commercial cantilever (BL-AC40TS, Olympus, Japan) with a nominal spring constant of < 0.09 N/m was used. Utilizing such a cantilever with a small spring constant allows for a relatively large deflection with the application of a small force and allows for reliable data collection of the cell surface structure. Spring constant calibration of the AFM cantilever was performed using the thermal vibration method. Measurements were performed using 50 forces curves containing 512 data points each (Figure 1a). To analyze the force curves, a Hertz model was implemented using the Park Systems imaging analysis program (Park XEI, Park Systems). The shape of the AFM tip was assumed to be a four-sided pyramid with half cone angle α. As a result, the force (F) applied on the cantilever is expressed as:

$$F = \frac{E}{1-\nu^2}\frac{\tan\alpha}{\sqrt{2}}\delta^2, \quad (1)$$

Where E is the Young's modulus, v is the Poisson's ratio and δ is the indentation (depth). Poisson's ratio was set to 0.5 and α was set to 35°. The AFM scan rate was set to 1μm/s and the maximum loading force was 8 nN.

SICM measurement for cell imaging and fluctuation analysis

SICM utilizes an ion current that flows between an electrode placed inside a nano-pipette and an external electrode located in a bath solution (Figure 1b). The ion current provides a feedback signal that regulates a constant tip-to-sample distance and allows the nano-pipette to scan topographical information. Despite having low lateral resolution (~30 nm) [7], SICM can display useful topographical measurements without the need to apply mechanical forces onto the sample surface. Figure 2 shows the height images of the live and fixed L929 cell. At first glance, there is no difference between two cases; however, the surface of the fixed cell is slightly rougher due to cross-linking of cell membrane proteins.

To perform SICM imaging and ion current-distance (I-D) curve experiments, 80 nm inner diameter nano-pipettes were fabricated from borosilicate capillaries (inner diameter 0.6 mm, outer diameter 1.0 mm, World Precision Instruments, SSA) using a CO_2-laser pipette puller (Sutter Instruments, USA).

Results and Discussion

Young's modulus of live and fixed cells

To determine the stiffness of live and fixed cell surfaces, force spectroscopy measurements were obtained from live cells, fixed cells as well as a solid substrate and those force-distance curves are shown in Figure 3a. Fixed cells show a significantly steeper force curve slope compared to that of live cells. Additionally, the force required for surface indentation is also greater for fixed cells than

for live cells. Table 1 presents the average Young's modulus values which indicated that the stiffness of fixed cells (77.95 kPa) was greater than live cells (8.11 kPa). These AFM cell stiffness measurements suggested that the acting filamentous structures strongly affected the stiffness. Another notable mention is that PFA treatment affects the cross-linking of cell surface proteins, including F-actin filaments. In addition, it was noted that cell stiffening corresponds to protein cross linking [8]. More specifically, the PFA fixation process can be assumed to have a direct link to an increase of cell stiffness depending on the number of randomly distributed cross-linking sites available on the cell surface [9].

Surface fluctuations of live and fixed cells

To obtain cell surface fluctuations, the I-D curves were obtained using SICM measurements on live cells, fixed cells and a solid substrate. I-D curves exhibit the steepest slope for solid substrates (petri dish) while untreated they possess a broader slope. For PFA-treated cells, I-D curves occur amidst the two. Subsequently it could be concluded that the live cells demonstrated more activity compared to fixed cells. The PFA treatment process results in smaller surface fluctuations for fixed cells which results in cross-linking of proteins between the membrane and cytoplasmic proteins.

Conclusion

A fundamental mechanical difference has been demonstrated by comparing live cells and cells fixed with PFA. Atomic force microscopy and scanning ion conductance microscopy measurements revealed a definite transition in surface fluctuation and elastic modulus of cells when exposed to PFA. Proceeding complete fixation with PFA, cell surface fluctuation decreased as compared to a live cell while the Young's modulus increased by five-fold. These findings provide key insights into how cells react to chemical treatment with PFA. In addition to the traditional knowledge of the chemical influence of PFA on cells, this study has uncovered the effect of PFA on the mechanical properties of the cell's surface. Cell membranes are assumed to be flexible and variable; however, in certain situations (chemical treatment in particular), transformations occur on biological and morphological levels. Such observations provide a strong motive for further study on cell surface fluctuations as a crucial requirement for the understanding of cell functions regarding cell dynamics. Scanning probe microscopy techniques, specifically the AFM and SICM, clearly serve as vital tools in the application of quantitative studies on both fixed and live cells.

Figure List

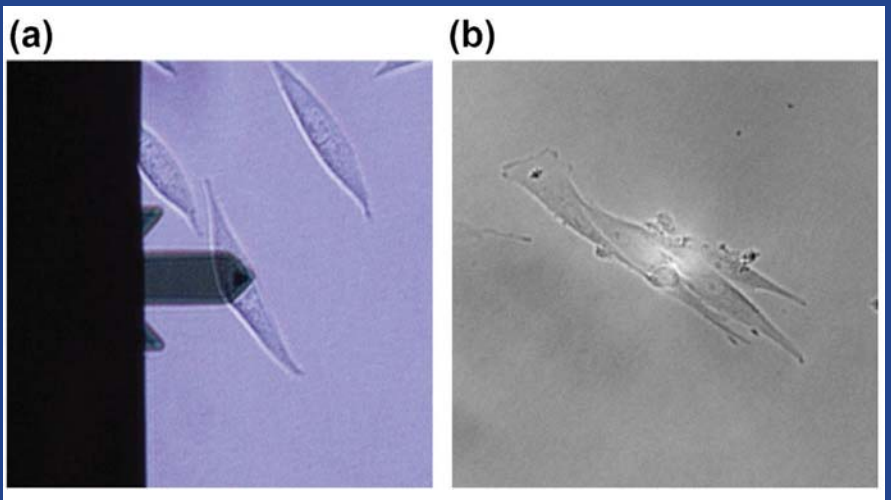

Figure 1. Optical images of L929 cell for AFM (a) and SICM (b). Each probe was positioned at the apex of the single cell.

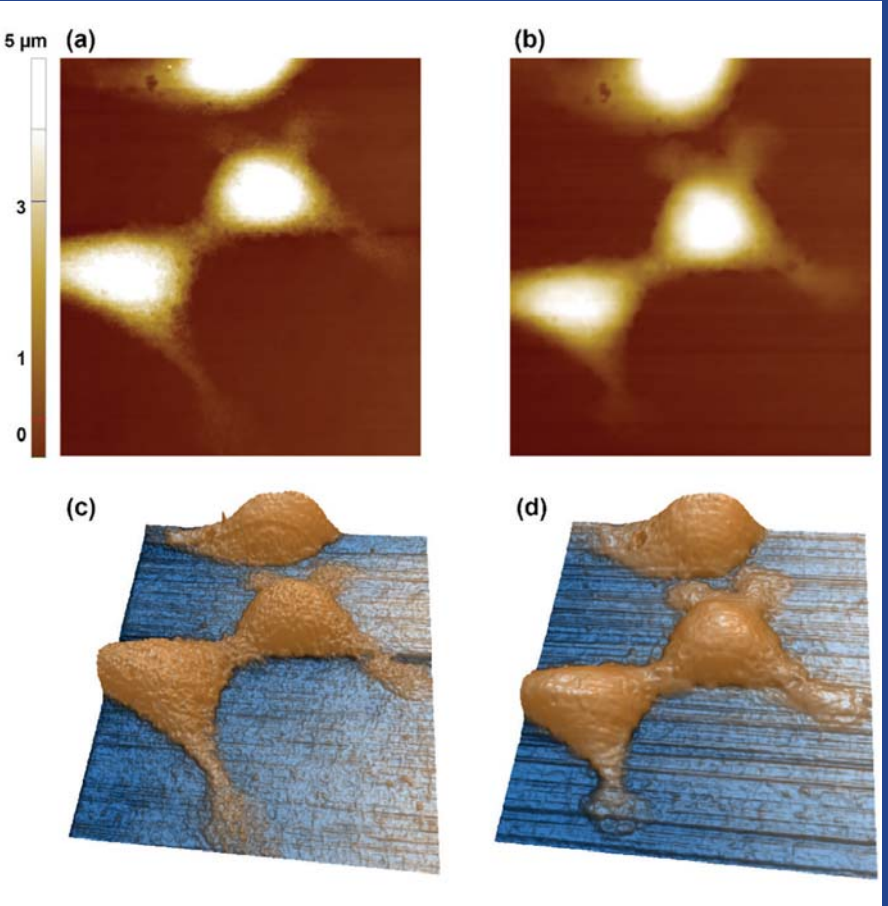

Figure 2. Live (a),(c) and 4% PFA treated (b),(d) cell surface imaging by SICM.

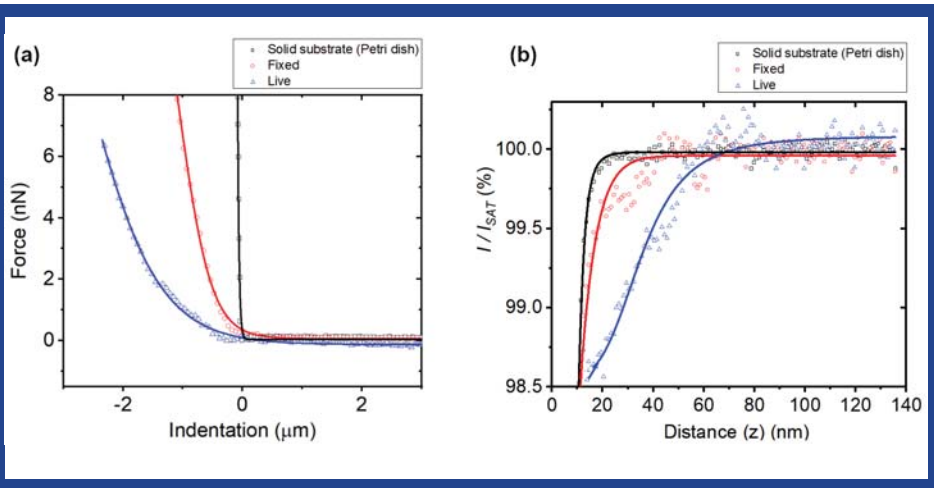

Figure 3. Average force-distance curves (a), and ion-current-distance curves (b) of the solid substrate (black), 4% PFA treated (fixed) cell (red) and live cell (blue).

Table 1. Young's modulus values.

Paraformaldehyde Concentration (%)	Young's Modulus	
	Mean	SD
Live cell (0)	8.11 kPa	2.93
Fixed (4)	77.95 kPa	8.16

References

[1] Lanier, L. and N. Warner, Paraformaldehyde fixation of hematopoietic cells for quantitative flow cytometry (FACS) analysis. Journal of immunological methods, 1981. 47(1): p. 25-30.

[2] Yamane, Y., et al., Quantitative analyses of topography and elasticity of living and fixed astrocytes. Journal of electron microscopy, 2000. 49(3): p. 463-471.

[3] Binnig, G., C.F. Quate, and C. Gerber, Atomic force microscope. Physical review letters, 1986. 56(9): p. 930.

[4] Korchev, Y.E., et al., Scanning ion conductance microscopy of living cells. Biophysical journal, 1997. 73(2): p. 653.

[5] Cappella, B. and G. Dietler, Force-distance curves by atomic force microscopy. Surface science reports, 1999. 34(1): p. 1-104.

[6] Mizutani, Y., et al., Nanoscale fluctuations on epithelial cell surfaces investigated by scanning ion conductance microscopy. Applied Physics Letters, 2013. 102(17): p. 173703.

[7] Rheinlaender, J., et al., Comparison of scanning ion conductance microscopy with atomic force microscopy for cell imaging. Langmuir, 2010. 27(2): p. 697-704.

[8] Hopwood D. Theoretical and practical aspects of glutaraldehyde fixation. In Fixation in histochemistry, Springer, Boston, MA. 1973: p. 47-83.

[9] Tanaka KA, et al., Membrane molecules mobile even after chemical fixation. Nature Methods. 2010 Nov;7(11):865.

NANOSCIENTIFIC BREAK-THROUGHS

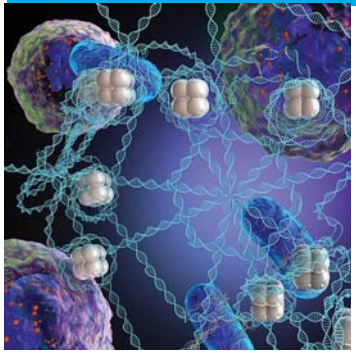

Engineering DNA to Mimic Biology - Creating a Web to Trap Bacteria Using DNA at Georgia Tech Nature inspired this synthetic microweb that nabs bacteria and allows antibiotics to more effectively kill them. White blood cells shoot so-called NETs like Spiderman at bacteria. NETs contain hundreds of ingredients, the main one being DNA, but researchers engineered their microweb with just DNA and one other ingredient. Credit: Georgia Tech / Ella Maru Studio

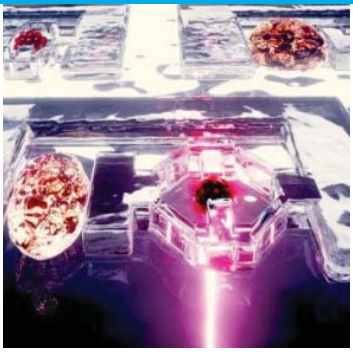

Tiny Gel Robots Wirelessly Activated by Laser Beams to Prevent Disease at Ecole Polytechnique Fédérale de Lausanne- micromachines able to mechanically stimulate cells and microtissue. These tools, which are powered by cell-sized artificial muscles, can carry out complicated manipulation tasks under physiological conditions on a microscopic scale.

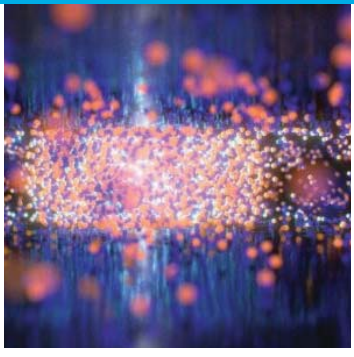

Creating the first 'electron liquid' by bombarding an ultrathin semiconductor sandwich with powerful laser pulses at University of California - By bombarding an ultrathin semiconductor sandwich with powerful laser pulses, physicists have created the first 'electron liquid' at room temperature. The achievement opens a pathway for development of the first practical and efficient devices to generate and detect light at terahertz wavelengths -- between infrared light and microwaves.

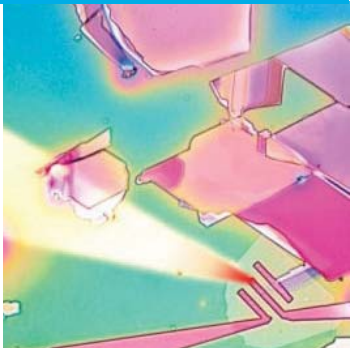

Fabricating Atom-thin processors to Reduce Cost on Electron beam lithography at New York University Tandon School of Engineering- Researchers reported that lithography using a probe heated above 100 degrees Celsius outperformed standard electron beam lithography for fabricating metal electrodes for promising 2D semiconductor materials such as molybdenum disulfide.

COLUMN 1

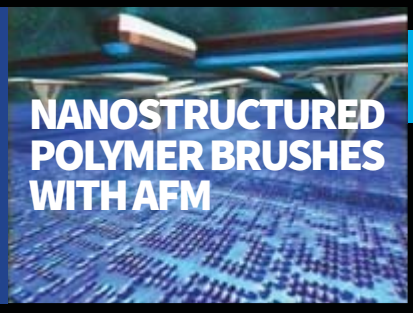

NANOSTRUCTURED POLYMER BRUSHES WITH AFM

MATERIALS MATTER

Column Highlighting Topics Presented in Dr. Advincula's Monthly Webinars on Advancements in Material Science

What are nanostructured polymers and what applications are they used for?
Coatings are very important industrial applications of materials for protecting, packaging, and labeling. It is important to develop smart coatings that go into various products that enhance performance. Bulk coatings can come in the form of paint or protective coatings. On the other hand, ultrathin or even layered coatings are important in methods for makings flexible electronics, display devices, solid state devices, and sensors. The grafting of polymers and substrates enable surface modification that allow nanostructuring based on composition and ability to stretch the chain perpendicular to the grafting substrate. Polymer brushes indicate high grafting density on surfaces, whether it is flat substrate surfaces or irregular and spherical objects. A polymer brush then has the ability to expose the end groups or modulate transport through the film. This makes them useful as barrier materials or enhancement of lubrication. They can also be designed as sensors.

How are AFM used in conjunction with nanostructured polymer brushes and why is AFM an important tool for this application?
There are many other methods that have been used to characterize thin films including optical microscopy, electrochemistry, optical ellipsometry, etc. However, one of the best ways of characterizing these films is through surface probe microscopy (SPM) and best exhibited by AFM with various enhanced methods. AFM is a vital tool in characterizing the morphology of these grafted polymer brushes and the use of modified techniques to enhanced surface probing. This includes surface tribology, thermal field enhancement, electrostatic chargers,etc. which can be built into the tip design or the experimental design. The use of surface probe methods enable a better understanding of the effect of polymer density on the behavior - even stimuli-responsive behavior of the brushes.

How is Park Atomic Force Microscope (AFM) specifically used in this application and which features are most useful of Park AFM?
Park AFM is an outstanding SPM instrument and technique (methods development) to probe polymer brushes. The XY and Z decoupling and cantilever tip positioning will enable imaging beyond that of idealized flat film surfaces. Park AFM has developed a number of tools and techniques to probe these surfaces namely> Electrostatic mode, lateral force microscopy, current sensing AFM, indentation methods, etc. to enable elucidation of structure-composition-property relationship in these films.

What is a Polymer Brush?
By definition, we can say that a polymer brush is a polymer chain that is tethered to a surface or interface with a sufficient surface density such that the polymer chains are forced to stretch away from the surface to avoid crowding. This can also be represented by a grafting density that is much smaller than the radius of gyration.

The term polymer brush of course is analogous to a brush, a brush where you have extended bristles or chain but in this case, we're talking about in macromolecular level. There are a number of methods for tethering polymers on surfaces. We can simply classify them as a physical or a chemical adsorption method. What we label physical adsorption means that you have an interfacial boundary where a block of polymer or surfactant is distributed between these boundaries of two faces. It can be achieved thermally or solvolytically. However, these are initially non-equilibrium phases which then equilibrate overtime. One of the consequences here is that since they are not a chemical boundary of realize that the ordering at the interface with the equilibrium, they do not easily achieve very high grafting densities.

One the other hand, what we call chemical adsorption usually results in a covalent bond formation or tethering chemistry which can be achieved by let's say silane chemistry or phosphoric acid chemistry on metals or oxides or the interaction of thiol on gold. This means the adsorption can be achieved at a boundary, a surface, or an interface where this chemical adsorption or chemical interaction takes place.

Can you describe Grafting Methods for Polymer Brushes?
To distinguish grafting methods based on either physisorptions and chemisorptions, we call a "grafting on to" approach where we have an existing polymer chain with a group that is chemically or physically bound to a surface. Where we do polymerization such that the initiation takes place in the bulk during polymerization, it stitches through or grafts through surface bound monomer species, there we have a "grafting through" process. However, what perhaps enables the formation of high grafting density chains better than the first two is what we call "grafting from" method or surface-initiated polymerization method.

What is surface-initiated polymerization?
It represents a grafting as I mentioned wherein the grafting point is much less than the radius of gyration. This simply means that an initiator in an addition polymerization method typically are like free-radical, ATRP, RAFT, cationic, anionic, or metathesis polymerization originates from the surface. In other words, the initiator is bound on the surface and the monomer is limited by its diffusion to the surface. Hence, it affects the polymerization kinetics dramatically. This can be done on a flat surface, a colloidal particle surface, or other types of interfacial boundaries.

What is a General Strategy for SIP?
The initiator is first immobilized on the surface. After immobilization of the initiator with a specific density, then polymerization takes place. Polymerization takes place where you have the active monomer, diffusing to the surface and then as the polymer grows, there's crowding out of the interface. One of the challenges of a grafting from technique is actually diffusion of the monomer and the crowding out of the interface or surface, sometimes leading to inefficiency or non-initiation of the surface bound initiators.

Why do you use Surface Initiated Polymerization Instead Of "Grafting To"?
In a "grafting onto" method, the polymer approaches from the bulk interface or solution which can be achieved by physisorption or chemisorption method of course. That means that the pre-existing polymer with its

given molecular weight, polydispersity, and availability of the reactive group or physically adsorbing group has to find its way at the interface. Hence, some of the challenges of a "grafting to" approach is that of achieving of a very high grafting density. It is also of course related to the different regimes by which a polymer or a grafted polymer falls on to in its certain stages of equilibrium.

Can you show how Microchemical and Lubrication Properties Are Probed By Atomic Force Microscopy?

Here is one interesting example which shows that the micromechanical and lubrication properties of a surface can be changed as well by the condition as well as the patterning on a surface. What we have here is basically a polymer in which we have different charge densities and regimes. Depending on the type of solvent, it will have a variety of friction, force, properties on a surface. Dry state or swollen state for example can cause changes on the height of this polymer brushes and hence affects them of its wetting behavior.

Just to emphasis this fact, let's say, a very well known lotus effect in nature that is copied on surfaces can of course affect new wetting behavior of a tethered polymer system or the morphology of a particular thin film as well as the formation of different types of lithographically bound surfaces enhance the wetting behavior. Most of this is in fact characterized by the Cassie-Baxter phenomenon.

Can you describe your work with Polymer Brushes?

So back in 2006, we actually published one of the first books on grafting polymer brushes and monographs as well have appeared. This technology is about 25 years old in terms of its potential uses in fields like electronic devices, wetting, packaging, and biomedical applications. What I would like to emphasize are some of the chemistries that we've developed through the years involving that of polymer brushes based on surfaces. We are one of the first to pioneer what we call anionic polymerization on surfaces. We call this the LASIP technique. One technique that we use involves the tethering of diphenylethylene co-initiators which were then activated by n-Butyllithium. The anionic anion generated allows us to, for example, polymerized thyrine or even form a block of polymer brush with isoprene. Hence, in a classical anionic polymerization which is done in solution, we're able to do it on surfaces, and in this case, a modified bulk surface with a diphenylethylene co-initiator.

Some of these early works resulted in the following. We were able to control the grafting of these polymers actually on silicon wafer and bulk surfaces as well. This was done by using n-Butyllithium on the diphenylethylene initiator and for example, the left AFM picture shows the graphic on a silicon wafer surface and the right one on a gold-coated wafer, which actually showed a thicker brush of about 23 nm versus 13.7 nm.

We were able to graft polystyrene and then followed by a grafting of isoprene. This is a living anionic polymerization, after depleting all the styrene monomers, we simply add in the isoprene monomer to produce these block copolymers not only with isoprene, we were able to achieve this with blocks of polystyrene and polyethylene oxide and polyisoprene and PMMA.

What are the General Stages of SIP on Particles?

Particle polymerization simply means that the grafting is done again by tethering the initiator on the particle with a number of strategies outlined earlier, chemisorption or even physisorption, and then followed by the polymerization in the particle. What happens is we achieve a core-shell geometry where the core is the particle substrate and the shell is the grafted polymer brush.

What we would do in a typical procedure is actually through a characterized the grafted polymer using SEC. For example, if we use silica particle as a substrate, we would then mix it with potassium hydroxide, alcohol to remove the bulk polymer. The bulk polymer can then be characterized normally by GPC.

What we found actually on this LASIP procedure is that we were able to get a good correspondence of the monomer styrene feed ratio with the molecular weight of the polymer, hence, we actually achieve here a type of living polymerization. However, not the exact monomer feed ratio but in terms of the linearity of the process, it is well taken.

We have also done this on clay nanoparticles. We modified clay with a cationic diphenylethylene initiator, activated with n-Butyllithium. What's interesting with clay is that of course it is hydroscopic and therefore, by heating it up and drying it a 120° C which is a very important procedure, we were able to do anionic polymerization on clay with that cationic bond surface initiator. Characterization can be done by infrared spectroscopy both for the polymer bound on the clay or separate it from the polymer after they're grafted. Interestingly, since the polymerization is followed by the intercalation and delamination of the clay platelets, then we can also observe the changes that are happening on this space in between each of those clay platelets by x-ay diffraction.

What are Nanostructured Layer-by-layer Self-assembly?

The use of polyelectrolytes to modify surfaces with charge particles or polyelectrolytes can be achieved by alternating the deposition of let's say a negatively charged polyelectrolyte and a positively charged polyelectrolytes. This can be done on a flat surface or a particle surface. You can achieve in fact, a hollow shell configuration by removing the particle. This has been done by many, many groups through the years and demonstrated in particles and surface substrates as well. We have done a lot of work in this field through the years.

How are Polymer Brushes used for Application in PLEDs?

It is interesting to point out the use of Polymer brushes as applied to solid state devices and polymer brushes patterned on interfaces using colloids and polymer grafting methods. One of the interesting things with solid state devices is trying to play an important role of the cold transport or even electrode transport in devices such as LED and photovoltaic devices. Polymers play a very important role whether it's the active material or the passive material. Another interesting area is the patterning, specifically Electrochemically Grafted Macroinitiators and Conducting Polymer Films. In the webinar, I give many examples of this including the technique of electropolymerization to graft a RAFT (reversible addition-fragmentation chain transfer) initiator on a conducting surface, Electropatterning of Binary Polymer Brushes by Surface-initiated RAFT and ATRP, Fabrication of Patterned Binary Brushes of PS and PNIPAM, FT-IR Imaging of PS-PNIPAM Patterned Brush and Patterned Surfaces Combining Polymer Brushes and Conducting Polymer via Colloidal Template Electropolymerization.

We have also patterned polymer brushes using colloidal templates. Back in 2011, we demonstrated that colloidal particles can be used to patterned surfaces where the colloidal particles can form a hexagonally patch structure as shown here. The interstitial spaces provides a way for electrodeposition let's say a conducting polymer to be made on the electrode surface. Hence, by masking or using this as templates, one can observe the formation of arrays as shown here. These arrays are conducting polymers that were deposited at the interstitial spaces in between those of the particles resulting in a honeycomb, half comb, or full dome structure as shown here. In fact, they can be harvested even as particles.

Please explain Electro-Patterned Polymer Brushes via Electrodeposited ATRP Initiator and Colloidal Templating.

We can actually grow the polymer brush along the arrays. In this case, after electrodepositing this macroinitiator of the surface, the colloidal particles were then removed revealing a macroinitiator surface and then growing the polymer brush. We were able to demonstrate this with an ATRP, RAFT and a metathesis system. Just to show you all three, we were able to do the grafted polymer system. You can see the change in morphology by AFM as we grow the polymer brushes along the ridges of the patterned array, not in the hole. On the other hand, since we are able to do modify the hole with an initiator for ATRP, we can do a dual or binary composition in which the arrays are modified with a polymer brush, but then we can also modify the holes with another polymer brush having a binary composition. In fact, we were able to characterize this place on the diffusion properties of let's say a molecular ion probe using cyclic voltammetry as a method to look at the diffusion of polymers on a conducting substrate.

For the complete webinar on Nanostructured Polymer Brushes and to register for the series, go to:http://parksystems.com/webinar2019

Beginning on Jan. 16, 2019, Park Systems began offering a new free webinar series titled "Materials Matter" by Dr. Rigoberto Advincula, Professor, Department of Macromolecular Science and Engineering at Case Western Reserve University and editor-in-chief of MRS Communications, Materials Research Society. A new webinar covering leading edge developments in Materials Science Research and applications using AFM will be presented every third Wed of the month at 12pm EST for the entire year. Each issue of NanoScientific will offer a column highlighting one of the lectures.

Dr. Rigoberto Advincula

Dr. Advincula is a professor of Macromolecular Science and Engineering at Case Western Reserve University and Editor-in-Chief at MRS Communications. He's a Fellow of the American Chemical Society and a Humboldt Fellow among many other professional awards, published more than 250 peer-reviewed publications, and a particular note for today's topic is the co-editor of the book "Polymer Brushes, Synthesis Characterization and Applications".

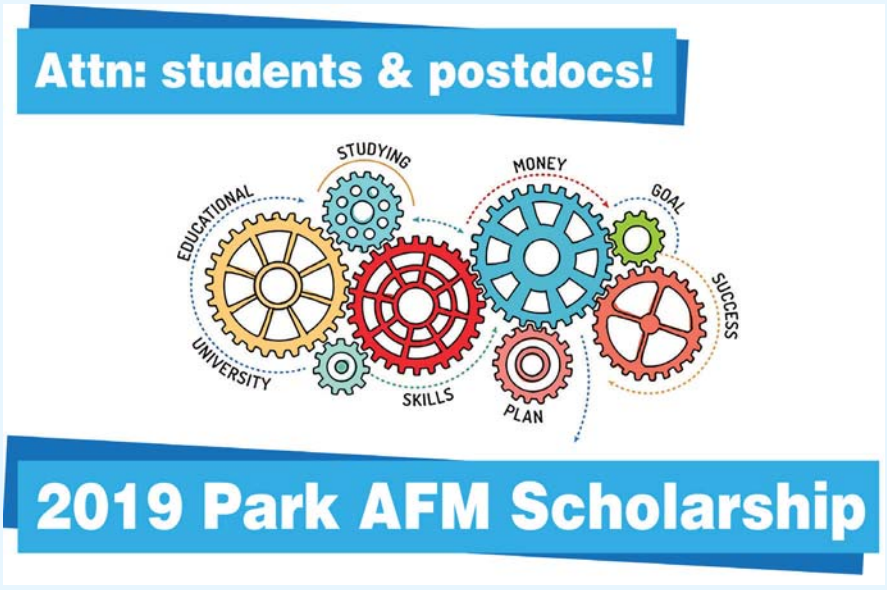

Park Systems Park AFM Scholarship Awards

Program currently open to ALL regions around the world

Park Systems, the world's leading manufacturer of atomic force microscopes (AFM) invites all researchers worldwide to apply to become Park AFM Scholars and receive a research scholarship. Park AFM Scholarship Awards are open to undergraduate or postdoctoral students working in nanotechnology research either already using Park AFM or who have research they would like to do with a Park AFM and need help getting access to equipment. Through this program, Park Systems has offered assistance to many researchers who qualify as Park AFM Scholars by matching them with one of thousands of nanoscience shared user facilities to perform their research using Park AFMs.

The Park AFM Scholarship Award is open to postdoctoral researchers and graduate students working in nanotechnology research using Park AFM. As progress for nanotechnology research and development advances at an unprecedented rate, universities worldwide offer degrees in fields working with nanotechnology. Park Systems, world-leading manufacturer of atomic force microscopes, is offering a $500 USD monetary scholarship to promote the education of future scientists and engineers in a number of nanoscience research areas that require advanced nanoscale microscopy for sample analysis and observation and to promote shared research findings and methodologies amongst their peers.

PARK AFM SCHOLARSHIP PROGRAM ACCEPTING SUBMISSIONS

Park Systems is continuing their successful Park AFM Scholarship Program.

To be eligible:

1) The awardee must be a graduate student or postdoctoral researcher currently enrolled/affiliated with a research university, national laboratory, or governmental agency.

2) The research being presented must include meaningful data acquired using a Park AFM instrument. This data can either be the sole data being discussed in the presentation or be in conjunction with data acquired with other types of tools.

Park Systems will offer assistance to researchers who need a facility to perform their research using Park Atomic Force Microscope by matching them with one of their shared nano facilities.

For more information on the Park AFM Scholarship program, go to:

https://www.parksystems.com/index.php/medias/programs/park-afm-scholarship

Park NX12

The most versatile atomic force microscope for analytical chemistry

- ***Built on proven Park AFM performance***
- ***Equipped with inverted optical microscope***

Proven Performance
The Park NX12 is based on the Park NX10, one of the most trusted and widely used AFMs for research. Users can rest assured that they are taking measurements with a cutting-edge tool.

Built for Versatility
Multi-user labs need a versatile microscope to meet a wide range of needs. The Park NX12 was built from the ground up to be a flexible modular platform to allow shared facilities to invest in a single AFM to perform any task.

Competitive Pricing
Early career researchers need to do great work with cost-effective tools. Despite its outstanding pedigree, the Park NX12 is priced affordably—ideal for those on a constrained budget.

To learn more about Park NX12
Please visit parksystems.com/nx12 or email: inquiry@parksystems.com

Park SYSTEMS
parksystems.com